DETECTION OF EARLY CHANGES IN WHITE MATTER DEGENERATION USING TEXTURE ANALYSIS OF MAGNETIC RESONANCE IMAGES

by

Debosmita Biswas

A Thesis
Submitted to the
Graduate Faculty
of
George Mason University
in Partial Fulfillment of
The Requirements for the Degree
of
Master of Science
Electrical and Computer Engineering

Committee:

V Ikonomidou	Dr. Vasiliki Ikonomidou, Thesis Director
	Dr. Kenneth J. Hintz, Committee Member
	Dr. Siddhartha Sikdar, Committee Member
	Dr. Andre Manitius, Chair, Department of Electrical and Computer Engineering
Kenneth S Ball	Dr. Kenneth S. Ball, Dean, Volgenau School of Engineering
Date: July 24 2013	Summer Semester 2013 George Mason University Fairfax, VA

Detection of Early Changes in White Matter Degeneration Using Texture Analysis of Magnetic Resonance Images

A Thesis submitted in partial fulfillment of the requirements for the degree of Master of Science at George Mason University

by

Debosmita Biswas
Bachelor of Science
University of Mumbai, 2007

Director: Vasiliki Ikonomidou, Assistant Professor
Department of Electrical and Computer Engineering

Summer Semester 2013
George Mason University
Fairfax, VA

DEDICATION

Dedicated to my parents and my husband Ashis.

ACKNOWLEDGEMENTS

I want to express my heartfelt appreciation and sincere gratitude to Dr. Vasiliki Ikonomidou for providing me with this wonderful opportunity to conduct research under her friendly guidance. Her wonderful analytical skills, and cool and calm composure has made this an unforgettable learning experience. I am sure this will stand me in good stead in my future professional career. I would also like to thank Dr. Hintz and Dr. Sikdar for readily accepting to be in my thesis committee.

I am thankful to George Mason University (GMU), Fairfax, Department of Electrical and Computer Engineering and The Krasnow Institute for their support and facilities. I would like to take this opportunity to thank all the professors I have known at GMU for their invaluable guidance.

I want to thank all my close friends: Ashwini, Aveek, Abinash, Sudhanshu, Anindya, Mekhala, Pallavi, Simrit, Balaji, Vijay, Ketki, Jayesh, Anish, Nishant and many others for their advice and help.

Of course, this would have been unattainable without the support of my family. I can never thank Mamma enough for convincing my father to let me come to USA to pursue MS. Thanks to Dodo, my brother, and all my dear cousins for their friendly rebukes and loads of affection.

Last, but not the least, I want to thank the two most important men of my life. I have to give huge thanks to Ashis, my husband, for giving me constant inputs while writing the thesis and more importantly, for teaching MATLAB, and Baba, my father, for proof reading my thesis. Also, I can never forget the number of ways Baba devised to generate my interest in science while I was still a toddler. I would not have been able to enjoy this achievement fully without them.

TABLE OF CONTENTS

LIST OF TABLES

Table Page

LIST OF FIGURES

Figure Page

LIST OF COMMONLY USED ABBREVIATIONS

Magnetic Resonance Imaging ..... MRI
Alzheimer's Disease ..... AD
apolipoprotein E ..... APOE
Texture Analysis ..... TA
Spatial Dependence Matrix ..... SDM
Region of Interest ..... ROI
Voxel Based Morphometry ..... VBM
Angular Second Moment ..... ASM
Inverse Difference Moment ..... IDM

ABSTRACT

DETECTION OF EARLY CHANGES IN WHITE MATTER DEGENERATION USING TEXTURE ANALYSIS OF MAGNETIC RESONANCE IMAGES

Debosmita Biswas, M.S.

George Mason University, 2013

Thesis Director: Dr. Vasiliki Ikonomidou

In the absence of permanent cure, early detection and diagnosis of neurodegenerative diseases are of utmost importance to make use of palliative measures for enhancing the quality of life of millions of Americans. However, a large number of people are not diagnosed at an early enough stage where medications can delay the full onset of the diseases (NIA 2013). While various techniques to analyze brain images of subjects have been proposed to address this challenge, none of the techniques provide a robust and reliable solution. In this thesis, we present a novel technique using texture analysis of T_2 magnetic resonance (MR) images to lay the foundation for an effective solution, using Alzheimer's disease (AD) as the case study. The technique consists of the following four steps. First, we utilize the textural property of the MR images to obtain a set of features that encode statistically meaningful information about the spatial distributions of the gray tone variations. Second, we compute texture feature maps (a feature value stored at every image voxel) on the white matter regions of the images that

are segmented into regions of interest (ROIs) based on the anatomical structure of the brain. Third, we identify the subset of relevant and uncorrelated features from our initial feature set by using statistical measures like mean, coefficient of variance, and mutual information. These features yield statistically different values in the different ROIs and also in the different subjects for the same ROI, and the variations in the values are independent of each other. Thus, they are expected to afford better predictive powers in terms of detecting early signs of AD than the complementary set of features. Last, we validate the utility of the relevant features by carrying out statistical hypothesis tests on two groups of subjects, where the first group consists of subjects who have the APOE ε4 genes that are often found in AD patients, and the other group comprises of subjects who do not have the APOE ε4 genes. Results show that the entropy-type features yield promising results and are able to distinguish between the two types of subjects in many cases. It is hypothesized that the lack of statistical differences for certain subjects belonging to the two groups is due to the non-advent of neurodegeneration in those subjects. Hence, we believe that this technique provides a valuable first step towards early detection of neurodegenerative diseases without requiring genetic information and functional imaging modalities. Further work will involve more effective feature set generation and extensive validation and verification using ground truth information and long-duration trials involving monitoring of subjects who are predicted to have early symptoms of the diseases.

CHAPTER 1: INTRODUCTION

This Chapter is arranged in the following manner. Section 1.1 gives an overview of medical imaging in general and magnetic resonance imaging in particular, Section 1.2 discusses neurodegenerative diseases in general and Alzheimer's disease in particular, Section 1.3 presents the motivation behind the research undertaken in this thesis, Section 1.4 briefly discusses the research issues and Section 1.5 describes the outline of this thesis.

1.1 Magnetic Resonance Imaging

Medical imaging refers to the technique of creating images of parts of the human body for clinical processes, such as diagnosis and prognosis, or research studies. It differs from biopsy in the sense that organs and tissues do not have to be removed from the body. There are various methods for acquiring the images including radiography, magnetic resonance imaging (MRI), functional magnetic resonance imaging (fMRI), computed axial tomography (CAT), positron emission tomography (PET), scintigraph, single photon emission computed tomography (SPECT), ultrasonography (USG) etc. Measurement techniques that do not generate images, but produce data that can be represented as spatial maps like electroencephalography (EEG), magnetoencephalography (MEG), and electrocardiography (ECG), are also regarded as forms of medical imaging.

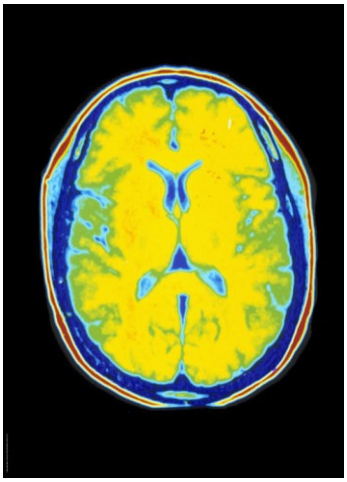

CT

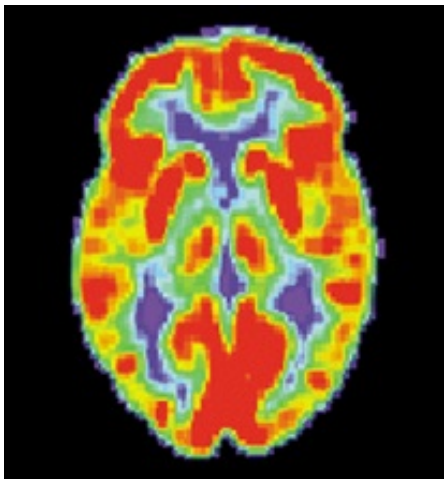

PET
image

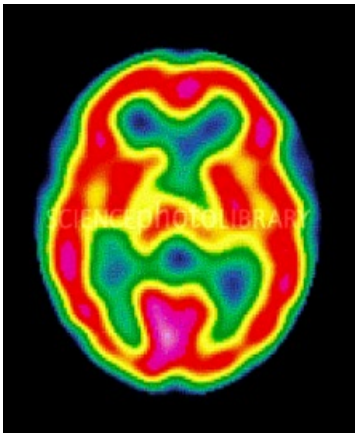

SPECT
image

Figure 1.1: Normal human brain using different imaging modalities (Image sources: http://cache2.allpostersimages.com/p/LRG/30/3040/5RSBF00Z/posters/human-brain-normal-ct-scan.jpg, http://upload.wikimedia.org/wikipedia/commons/2/20/PET_Normal_brain.jpg, and http://www.sciencephoto.com/image/307058/350wm/P3320430-Healthy_brain,_SPECT_scan-SPL.jpg)

Processing the acquired images, referred to as medical image processing, is currently one of the most potent tools to perceive and understand the healthy and pathological processes of a human body. Mathematically speaking, it amounts to the solution of an inverse problem, where the cause, namely the property of living tissue, is estimated or inferred from the effect measured from the observed signal. In particular, it is being used ubiquitously for understanding the structure and function of the brain. While structural imaging deals with the brain structure and is useful for the diagnosis of large-scale intra-cranial diseases and injuries, functional imaging attempts to understand the relationships between brain region activities and mental functions to diagnose diseases and lesions on a finer scale. Thus, functional imaging provides more information for the diagnosis of neurodegenerative diseases like Alzheimer's as compared to structural imaging at the expense of requiring more costly and sophisticated instrumentation. PET, fMRI, EEG, MEG, and SPECT are all types of functional imaging techniques or modalities, whereas CAT, MRI, and USG are examples of structural imaging modalities. Examples of the normal brain using three different imaging modalities, one structural and two functional, are shown in Figure 1.1.

MRI is one of the most commonly used techniques of brain imaging as it does not involve ionizing radiation (as for X-ray) or radioactive tracers (as in PET). Moreover, it provides better tissue contrast than both CAT and USG. It uses magnetic fields and radio waves to generate three-dimensional (3D) images of the brain by leveraging the phenomena of nuclear magnetic resonance in which the nuclei of atoms in the brain absorb and re-emit electromagnetic radiation at a specific resonance frequency in the

presence of a magnetic field, where the frequency depends on the magnetic field strength and the magnetic properties of the atom isotopes.

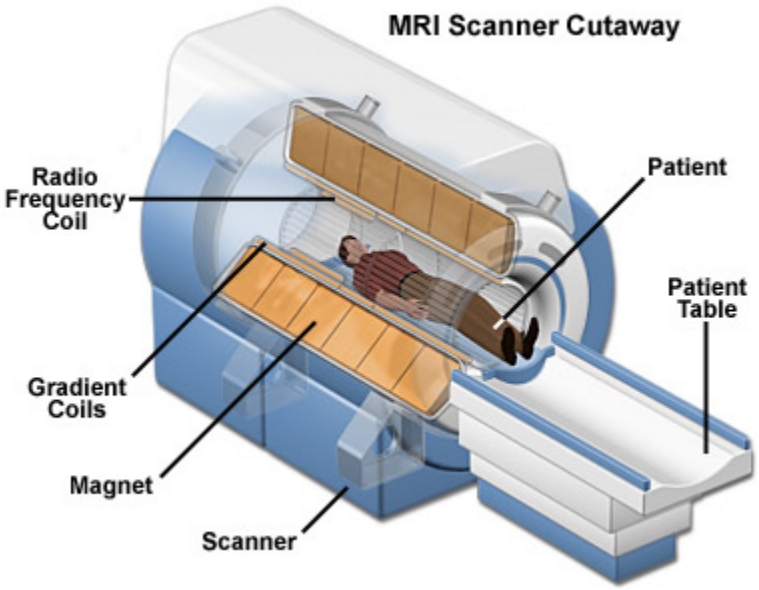

Figure 1.2: Schematic illustration of an MRI machine (Image source: http://www.magnet.fsu.edu/education/tutorials/magnetacademy/mri/images/mri-scanner.jpg)

MR imaging is performed by an MRI scanner, as shown in Figure 1.2, in which the subject is placed inside a large and powerful magnet that generates radio frequency magnetic waves with intensities of 1.5T to 8T for humans. When the subject is introduced in this field, the spins of the hydrogen nuclei protons that are present in the water molecules in the brain tissue align with the direction of the field of the scanner magnet. When the spins align, a magnetic moment is created parallel to the direction to the applied magnetic field. A radio-frequency (RF) pulse, of the same frequency as the

resonance frequency of the hydrogen protons, is then applied perpendicular to the scanner magnetic field. This causes absorption and flipping of the spins of the protons, resulting in tilting of the magnetic moment away from the magnetic field of the scanner. When the RF pulse is removed, the magnetic moment returns to thermodynamic equilibrium, i.e., it again becomes parallel to the magnetic field of the scanner. This process is called relaxation. During relaxation, the protons lose energy by emitting their own RF signals. This signal is called the free induction decay (FID) signal. The FID signal is measured by placing coils around the subject. This measurement is processed using Fourier transform to give MR images.

Different contrasts, such as T_1-weighted (or simply T_1), T_1 -MP RAGE, T_2-weighted (or simply T_2), T_2 -FLAIR, proton density (PD), and diffusion tensor imaging (DTI), are obtained by varying the RF pulse sequences, namely the pulse echo time and the inter-pulse repetition time. Specifically, in the case of the brain, T_1 images result in dark-colored cerebrospinal fluid (CSF), and T_2 images yield light-colored CSF with darker-colored white matter. Thus, T_1 images are useful for studying the normal anatomy, whereas T_2 images are well-suited for visualizing pathological anatomy (Butler et al. 2007). PD images show the CSF as very bright, with the gray matter being brighter than the white matter. The FLAIR contrast is most useful for examining the white matter plaques near the ventricles. fMRI measures the hemodynamic response (change in cerebral blood flow) related to any neuronal activity using the variation in the magnetization between oxygen-rich and oxygen-poor blood. Thus, it is most useful for understanding the functioning of normal, diseased, and injured brains by identifying the

regions that are closely associated with our critical functions such as speech, movement, sensing, and decision making. In summary, each of the contrasts gives unique information about the brain or a region of interest (ROI) therein. The variations in brain images using the different MR contrasts are shown in Figure 1.3.

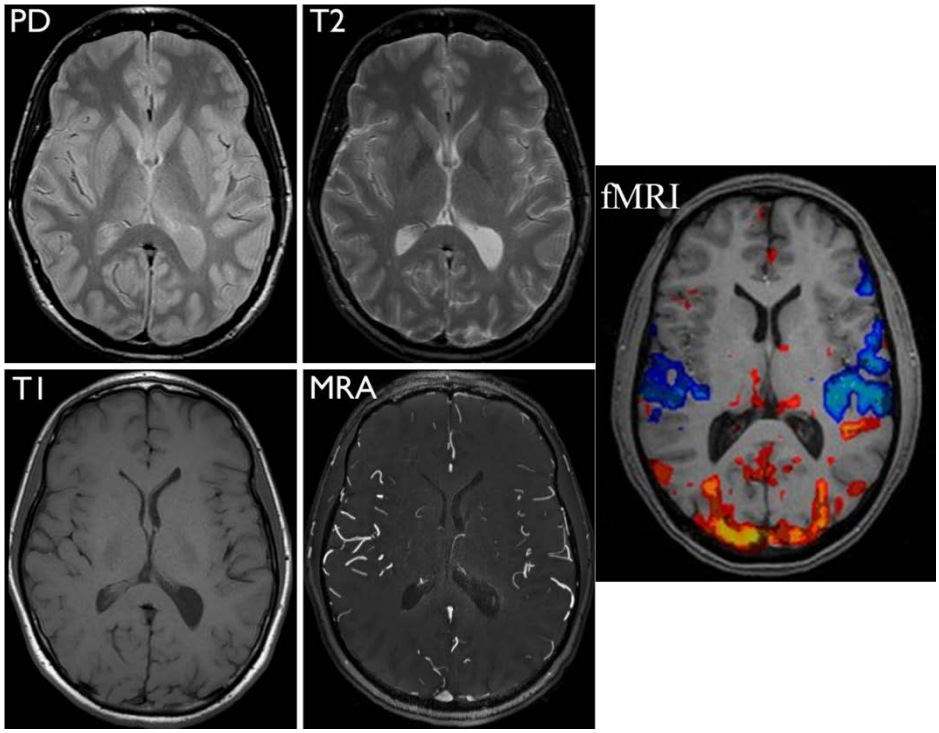

Figure 1.3: Normal human brain images using different MRI modalities (Image sources: http://blog.radiology.ucsf.edu/wp-content/uploads/2012/04/MRI_brain.jpg and http://psychcentral.com/lib/img/fmri_scan.jpg)

1.2 Alzheimer's Disease

Neurodegenerative diseases are increasingly becoming a severe cause for concern globally due to the rising number of patients, and worryingly, due to the lack of cure, effective diagnosis, detection, and knowledge of the reasons for occurrences. That is why, a lot of research is currently geared toward understanding the reasons and symptoms, and developing effective methods for early detection, diagnosis, and cure. In any neurodegenerative disease, there is a progressive loss of structure or function of neurons, eventually leading to their deaths. The four most commonly occurring forms are Alzheimer's, Parkinson's, Huntington's, and Amytrophic Lateral Sclerosis (ALS). Parkinson's disease manifests itself in the form of rigidity, resting tremor, and posture instability, and is caused by the deaths of dopamine-generating cells in the mid-brain region. Huntington's disease degrades muscle coordination and leads to cognitive decline and psychiatric problems; it is caused by an autosomal dominant mutation in either of the two copies of a gene named Huntingtin. ALS results in the degeneration of motor neurons selectively, which is believed to occur due to antioxidant enzyme Cu/Zn superoxide dismutase 1 (SOD1) mutations on astrocytes, the most abundant cells in the brain that provides biochemical support to endothelial cells, nutrients to the nervous tissue, extracellular ion balance, and repair following traumatic injuries.

Alzheimer's disease (AD) is the most commonly occurring neurodegenerative disease, which leads to dementia, a severe loss of global cognitive capabilities like memory, attention, speech, and decision making. In its early stages, AD results in difficulty in recollecting recent events. As it progresses, symptoms include aggression,

confusion, irritability, mood swings, and long-term memory loss. An estimated 5.4 million Americans suffer from AD (Alzheimer's Association 2012). The number is expected to increase as the number of people above the age of 65 increases. About two-thirds of all the people suffering from AD are women. The main reason is because women live longer than men. Other than that, there is no gender specific proneness. As with other neurodegenerative diseases, unfortunately, there is no permanent cure, and on an average, the life expectancy after diagnosis is only about seven years. Furthermore, diagnosis is very challenging due to the fact that the disease is somewhat different for every person and the symptoms are quite varied with many symptoms not clearly distinguishable from the effects of normal aging (Alzheimer's Association 2012).

From a neurological perspective, in the case of AD, the information transfer at synapses (nerve cell junctions) begins to fail and neurons start dying. As illustrated in Figure 1.4, the scans of patients with advanced AD show shrunken brains due to neuronal deaths. While the exact causes are not known definitively, it is believed that toxic changes occur in the brain during the pre-diagnosed stage due to abnormal deposits of proteins forming amyloid plaques and tau tangles (NIA 2013). Early-onset AD, which is a rare form of the disease that occurs in people belonging to the age group of 30-60, is believed to be caused by mutations in one of the three genes inherited from a parent. The much more predominant late-onset AD that affects people over the age of 60 has been linked to the apolipoprotein E (APOE) gene. In particular, APOE ε4 (to a large extent) and ε3 (to a smaller extent) gene forms (alleles) have been found to increase the risk of having late-onset AD (Farrer et al. 1997). More specifically, persons with the genotype

APOE ε4ε4 are at the highest risk for AD at an early age, followed by those with the genotype APOE ε3ε4. Persons with the genotype APOE ε3ε3 are considered to have normal risks, whereas those with genotype APOE ε2ε3 are regarded to have the lowest risks. It should be noted though that carrying this gene does not necessarily mean that the person will develop AD (NIA Genetics 2013).

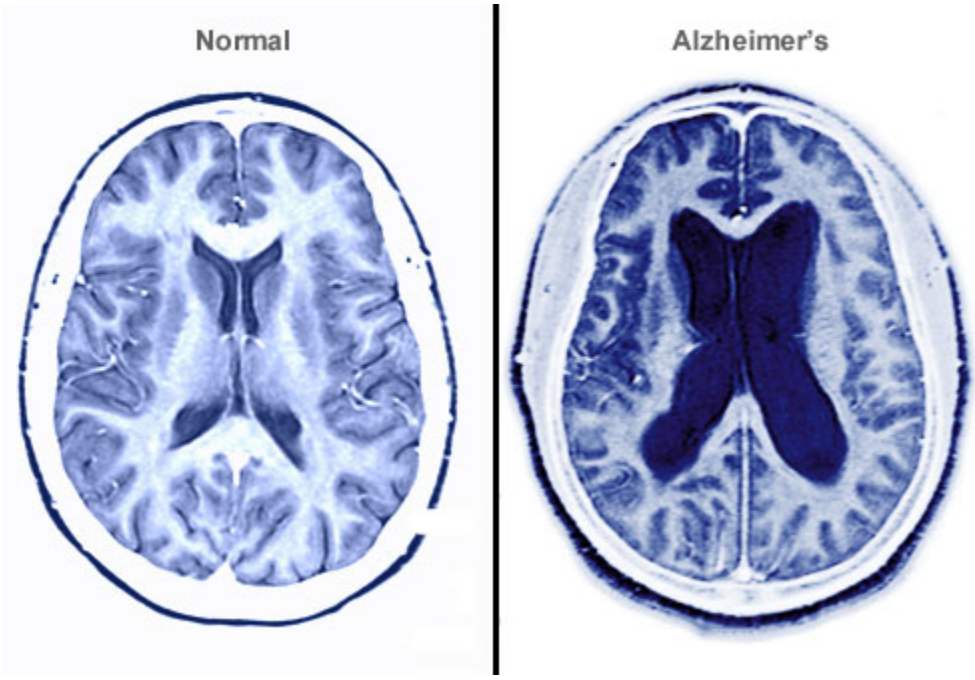

Figure 1.4: Comparison of MRI images of normal brain with AD brain (Image source: http://www.doctortipster.com/wp-content/uploads/2012/02/MRI-Alzheimer.jpg)

1.3 Motivation

Early detection of Alzheimer's disease using a combination of texture analysis and statistical testing of structural MR images: Detecting Alzheimer's disease before

clinically significant symptoms of decline start to occur in a patient is very vital. Medications such as cholinesterase inhibitors can then be prescribed that will delay the full onset of the disease. Such treatment gives the patients and their immediate family members time to plan for their futures (NIA Medication 2013).

It is clear from our discussion in Section 1.2 that there is a strong need to develop an effective and robust technique for early detection of AD in the pre-diagnosis phase during the formation of the abnormal protein deposits. To address this need, an exploratory study is conducted, wherein statistical metrics are applied to examine the degree of dependence between different texture analysis measures on T_2-weighted images from a dataset consisting of 26 middle-aged subjects (45-65 years old), all of whom have been genotyped for the APOE gene. The aim of this thesis is to possibly detect differences in white matter characteristics between the carriers and non-carriers of the APOE ε4 gene, a known risk factor for AD discussed in the previous Section. While the subjects are all neurologically healthy adults, they do show signs of early neurodegeneration in white matter regions of their brains (Ikonomidou et al. 2008), which in some cases reaches the point of gliosis. This white matter neurodegeneration provides a good range of variation for our data fitting and classification methods.

Following our discussion in Section 1.1, MRI is the best choice among the different structural imaging modalities due to its ability to provide good contrast between normal and pathological (lesion, plaque-filled etc.) tissue, and non-usage of ionizing radiation. Furthermore, T_2 is selected over other MR contrasts as it shows the white matter of the brain in darker shade as compared to other regions, thereby making it more

amenable for detecting early stage anomalies that typically occur in the white matter regions. fMRI and other functional imaging modalities are avoided to develop a technique that does not have to rely on the expensive, and, thus often unavailable or inaccessible, instrumentation and testing associated with such modalities.

Very slow deterioration of the brain tissue starts long before there are any apparent symptoms that can be associated with AD or any form of dementia. Unfortunately, detecting any change by direct inspection of a T_2 image is nearly impossible at this stage. However, statistical analysis of the pixel intensity distribution of the image can reveal the deteriorations (minute changes from normal brain tissue) where visual inspection is not helpful. (Herlidou et al. 1999, Bernasconi et al. 2001, and Mahmud et al. 2003). This image processing technique is referred to as *texture analysis*, which, thus, forms a suitable choice for detecting AD in its earliest stages. Other researchers have also started exploring texture analysis of T_2 -weighted MR images as a parallel and possibly complementary option to analysis of diffusion tensor images (Zhang, Brown, & Metz 2013).

Statistical measures are applied to ascertain trends and significant differences between the texture analyzed images of the subjects with and without APOE ε4 genes. Apart from examining the means and mutual information values of the texture maps, voxel-based analysis (VBA) is also used that involves processing and comparing images on a voxel by voxel basis. VBA is utilized as it provides better resolution than traditional morphometric methods that rely on volumetric calculations of large ROIs representing unambiguous structures such as hippocampi or the ventricles. However, there are a

number of morphometric features that may be more difficult to quantify by inspection, meaning that many structural differences may be overlooked. The benefit of VBA lies in the fact that it is not biased toward one particular structure and provides an even handed and comprehensive assessment of the anatomical differences throughout the brain (Ashburner and Friston 2000). In its basic form, any VBA method involves the following four steps: normalizing all the subject images in the same stereotactic space, segmenting and smoothing the gray matter segments, performing voxel-wise parametric statistical tests of the smoothed segments that are divided into groups, and performing corrections for multiple comparisons using Gaussian random fields.

Lastly, although the technique is validated by evaluating the differences in the processed images of subjects with and without the APOE genes, the technique itself does not use any genetic information. Thus, the technique can be used even when such information is unavailable, or as an additional measure of evaluating the onset of AD when such information is available since the presence of the APOE genes is not a guaranteed indicator of the future occurrence of AD.

1.4 Research Issues

There are two main research issues in addressing the problem discussed in the previous Section. They are described as follows:

- *Identification of features that encode meaningful information about the onset of Alzheimer's disease from MR images*: Identifying useful features or key attributes is always challenging for any real-world image processing problem. This identification

is usually done using a combination of feature selection and feature extraction. The former refers to the selection of a subset of features from much larger feature set, whereas the latter denotes the process of extracting features from the raw images using mathematical operations. Principal component analysis, independent component analysis, edge and contour detection, optical flow-based motion detection, thresholding, and Hough transforms are some of the common methods for feature extraction in image processing. While these methods work well for images of physical objects, they are found to be less useful for medical images. Instead, we will need to investigate alternative methods like texture analysis to provide a set of features that encodes relevant information about the intensity and contrast variations between healthy and AD-affected tissue. Henceforth, we will have to use statistical methods like mutual information as the evaluation metric to identify a smaller set of relevant features from the extracted feature set.

- *Validating the use of the identified features in providing statistically significant differences in certain brain region for subjects with and without Alzheimer's disease causing genes*: The primary challenge lies in obtaining the regions of interest (ROIs) where the identified features need to show statistically significant differences between subjects with and without the APOE ε4 genes. Based on the prior discussion that the effects of the onset of AD in the form of abnormal protein formation are expected to be more pronounced in the white matter region of the brain, we will investigate a suitable way to segment the brain into white matter ROIs based on anatomical

distinctions. Considering that such segmentation is already available for the standard brain atlas using T_1 MR images, we will need to develop a non-linear registration approach to first map the T_2 MR images of our subjects into the standard brain space before obtaining the desired ROIs. The actual validation step then has to be performed using a combination of two standard approaches: two-sample *t* test that is universally applied for testing whether the two sample means are equal, and voxel-based morphometry that is regularly employed in medical image processing for comparing images on a voxel-by-voxel basis.

1.5 Thesis Outline

The remainder of the thesis is organized as follows. Chapter 2 discusses the literature on medical image processing for early detection of neurodegenerative diseases. Chapter 3 describes the technical approach for detecting Alzheimer's disease using MR images. Chapter 4 presents the experimental results on a set of subjects divided into two groups based on the presence of APOE genes that are commonly associated with the Alzheimer's disease. Chapter 5 summarizes the conclusions reached from this research, highlights the anticipated benefits, and provides suggestions for future extensions of this work.

CHAPTER 2: RELATED WORK

This Chapter reviews the literature in the emerging field of processing MR images for early detection of neurodegenerative diseases. It is organized in the following manner. Section 2.1 discusses the works that perform texture analysis on MR images, Section 2.2 presents the literature on voxel-based analysis, Section 2.3 discusses the articles on using machine learning for image processing, Section 2.4 surveys the literature on other miscellaneous image analysis techniques, and Section 2.5 summarizes the successes and limitations of the existing methods.

2.1 Texture Analysis of MR Images

An early review of the role of texture analysis (TA) in medical image processing can be found in Castellano et al. (2004). The authors categorized the TA techniques into three types, namely, statistical (such as histograms and co-occurrence matrices), transform-based (such as wavelets), and model-based (such as auto-regression). They also discussed some of the successful applications of TA in segmenting anatomical structures, detecting lesions, and differentiating between pathological and healthy tissues in several human organs. A more recent survey of the advances in this field is given by Kassner & Thornhill (2010), where the authors also discussed the successful use of this technology in longitudinal monitoring of disease or recovery, and pointed out some of the common pitfalls in performing TA, and strategies on how to avoid them. A related

survey of the volumetric and TA-based techniques for early detection of AD in transgenic mouse models is provided in Muskulus et al. (2009).

The use of TA for early detection of neurodegenerative diseases using human brain images is a very recent and upcoming research area. Li et al. (2010) conducted a study on analyzing the hippocampus region using 4 textural features, namely energy, entropy, gray level nonuniformity, and run length nonuniformity, for three groups of subjects – AD patients, mild cognitive impairment (MCI) patients, and normal controls. The authors found that statistically significant differences existed among the AD, MCI, and normal controls for all the features except energy using the 3-way ANOVA test. They also observed that the texture features were correlated to the mini-mental examination scores, which suggested that these features could be used for describing the pathological changes in the hippocampus for early stage MCI and AD patients.

A related study was performed by Zhou et al. (2010) using three groups consisting of AD patients, elderly controls (ECs), and young controls (YCs). The results showed that significant differences existed between the AD and EC groups for three texture features, namely sum average, difference variance, and gray level non-uniformity. However, no significant differences could be found between the EC and YC groups for the same set of features. These results again indicated that texture analysis might capture the essential pathological changes in the hippocampus, thereby rendering it useful for early detection of AD.

A similar study was conducted on the corpus callosum of AD patients and normal controls (NCs) of different genders using 8 different textural features by Wang et al.

(2012). Statistical significance tests showed that the features were different not only between the AD and NC groups, but exhibited varying characteristics based on gender as well. These results indicated that gender-specific TA might be more useful for early detection of AD.

de Oliveira et al. (2011) computed a set of 11 textural features using co-occurrence matrices (COMs) after segmenting the corpus callosum and the thalamus regions of the human brain based on anatomical structures by manual mouse-clicking (the segments were later verified by a neurologist though). 4 different distances and angular directions were used to construct the COMs, resulting in a total of 176 textural descriptors for each segment or region of interest (ROI). The human subjects consisted of three types: those with amnestic MCI (aMCI), those with mild AD (mAD), and normally aging (controls). Pair-wise comparisons among the three groups using the Mann-Whitney *U* test showed significant differences between AD-control and aMCI-AD for the corpus callosum, and between AD-control, aMCI-AD, and aMCI-control for the thalamus segments.

Aggarwal & Agrawal (2012) compared the performance of 1^{st} and 2^{nd} order statistical texture features with wavelet-based features for classification of images into normal and AD groups with respect to sensitivity, specificity, accuracy, training, and test time. Experiments showed that the texture features outperformed the wavelet features when used in conjunction with any standard classifier such as support vector machines or *k*-nearest neighbors for all the performance metrics. These results further demonstrated the utility of TA as a valuable image processing technique for AD detection.

2.2 Voxel-based Analysis of MR Images

As discussed earlier in Section 1.3, voxel-based analysis (VBA) has emerged as a powerful technique over the past few years by providing better resolution than traditional morphometric methods that relied on volumetric calculations of large ROIs. We now discuss some of the representative works on this topic.

Stricker et al. (2008) used tract-based spatial statistics, wherein fractional anisotropy (FA) images are first computed from MR diffusion images to quantify the directionality of the local white matter tract structures, and a combination of non-linear registration and projection of FA images onto an alignment-invariant representation is performed for more accurate voxel wise comparisons across images. Experiments showed significantly lower FA in AD patients as compared to healthy older subjects in late-myelinating (inferior longitudinal fasciculus, superior longitudinal fasciculus) but not in early-myelinating (posterior limb of internal capsule, cerebral peduncles) fiber pathways. These results indicated that knowledge about white matter microstructural changes might provide valuable contribution toward early detection of AD.

Zhang et al. (2009) performed a similar analysis on FA images to distinguish between frontotemporal dementia (FTD) and AD (that is quite difficult to do clinically due to common symptoms) by identifying varying levels of white matter degradation. Experiments showed that FTD patients had reduced FA in frontal and temporal regions, whereas AD patients had reduced FA in parietal, frontal, and temporal regions as compared to normal controls. Furthermore, FTD patients showed greater FA reductions in the frontal region as compared to AD patients. Thus, the two results taken together

indicated that VBA might play a vital role in improving the diagnostic differentiation between FTD and AD.

Another similar study was conducted by Smith et al. (2010), who used VBA on FA images of two groups of women, one carrying APOE ε4 genes and having a family history of dementia, and the other without either of the two risk factors. Experiments showed reduced FA in several white matter regions for the first group.

2.3 Machine Learning-based Analysis of MR Images

Data classification forms one of the most fundamental and widely-studied problems in machine learning. Several supervised learning techniques, where training sets of correctly-labeled observations are available, such as support vector machines (SVMs), random forests (RFs), classification trees (CTs), boosting, and nearest neighbors (NNs) are commonly used for image classification, both at the overall scenario level and at the lower object or ROI level. Of late, these classifiers are being increasingly used for processing MR images to help in differentiating the key structural elements between healthy controls and those who already have or run the risks of having neurodegenerative diseases in the future. Representative works include the application of SVMs for separating the AD probable and normal controls by Duchesne et al. (2008), the combined use of RFs and SVMs in classifying the medial atrophy lobe regions to predict the probability of progressing to AD from MCI by Chincarini et al. (2011), the adoption of SVMs in classifying MCI patients from normal controls using a combination of MRI, FDG-PET, and CSF biomarkers by Zhang et al. (2011), and the use of a heterogeneous suite of classifiers in conjunction with mutual information-based feature selection to distinguish between healthy, MCI, and AD controls by Estella et al. (2012).

2.4 Miscellaneous Analysis Techniques of MR Images

Several other MR image analysis techniques that fall outside of the three broad categories discussed in the previous Sections have been used for early detection of neurodegenerative diseases. Most of these analyses are volumetric, while a few utilize other forms of geometric and topological information. Some representative volumetric works include the volume calculation method in predicting the progression from MCI to AD by Devanand et al. (2007), the use of medial temporal lobe morphometric measures such as entorhinal and perirhinal boundary thinning to differentiate between normal aging and onset of AD by Dickerson et al. (2009), the ventricular volume measurement method to demonstrate the complementary role of MRI and Pittsburgh compound B positron emission tomography in AD detection by Jack et al. (2009), the hippocampal volume estimation method to detect the onset of MCI and AD by Schuff et al. (2009), and the striatal and white matter region volume calculation procedure for early diagnosis of Huntington's disease by Paulsen et al. (2010). Representative non-volumetric works include the combined shape and probabilistic diffusion tractography-based connectivity analysis for thalamic degradation in AD patients by Zarei et al. (2009), and the anatomic segmentation procedure for healthy subjects, as well as MCI and AD patients, by Heckemann et al. (2011).

2.5 Summary

To summarize it can be said that the various image analysis techniques have shown promise in identification of neurodegenerative diseases in general, and AD in

particular, by identifying the differences in volumetric or morphological features between those carrying the risk of having AD in future or those who already have AD and healthy or normal controls. Interestingly though, the different techniques provide complementary capabilities, which implies that no single technique can be used profitably for the entire analysis sequence ranging from feature definition to image classification and comparison. While TA provides useful features containing statistically relevant information, VBA is suitable for final comparison of images based on the selected features, and the ML methods are designed for effective image classification into meaningful groups with varying feature levels. Thus, a hybrid approach that combines the key characteristics of multiple analysis techniques may lead to more accurate and robust detection of AD at the very early or potential risk stages.

CHAPTER 3: TECHNICAL APPROACH

This Chapter is arranged in the following manner. Section 3.1 describes the procedure for generating texture feature maps for T_2 weighted MR images that encode useful statistical information, Section 3.2 presents the procedure for computing the feature maps on segmented images where only the white matter is present for more accurate image clustering, Section 3.3 describes the technique for selecting the set of relevant features, and Section 3.4 presents the approach for statistical comparison of the white matter masked texture maps that are clustered into two groups, one for subjects with APOE ε4 genes present and the other for subjects with APOE ε4 genes absent, based on the relevant features.

3.1 Texture Feature Map Generation

Texture Analysis (TA) is used for recognizing valuable patterns in images as texture is an innate property of virtually all kinds of surfaces. It is observed in Castellano et al. (2004) that "Textural features contain information about the spatial distribution of tonal variations" within an image. We use a statistical approach to TA using the co-occurrence matrix (COM) or spatial dependence matrix (SDM) (Castellano et al. 2004, Haralick et al., 1973). The COM helps in extracting key statistical information or *features* from an image using the distribution of gray tones in pixel pairs. It is computed by defining a distance d and a direction θ, and analyzing the pairs of pixels that are separated

by this distance across the defined direction. A count is then made of the number of pairs of pixels that possess a given distribution of gray level values. For example, if a 4 X 4 image matrix has gray tone values of 0-3 as given by

technique that uses a combination of affine transformations, namely, translation, rotation, scaling, and shearing, to align one image with another.

2) Remove the non-brain tissue from

3.3 Relevant Feature Identification

We compute forty texture feature maps, one for each of the ten feature types and four SDM directions corresponding to a feature type, on every ROI of the white matter masked T_2 - weighted image. To facilitate the process of clustering the images of different human subjects based on whether early stages of AD are detected, we now want to identify the set of independent or relevant features. This identification is done in two ways. First, we compute the mean values of all the forty white matter masked texture feature maps for every ROI (each image voxel stores a particular feature value). We then observe the variations among the mean values both across all the different ROIs and across the four directions for a particular feature type. A feature, namely feature type – SDM direction pair, is termed as relevant if significant variations are observed across both ROIs and directions. The conclusion is strengthened by verifying that the corresponding standard deviation values are significantly smaller so that the coefficient of variation, given by the ratio of the mean and the standard deviation, is quite high (usually more than ten).

Second, we use the principle of mutual information. For any two discrete random variables X and Y, mutual information $I(X,Y)$ is given by

type and ROI. It is reasonable to assume here that the individual samples are independent, identically distributed, and drawn from two normal distributions. We use the Levene's test to first check the equality of the variances of the two samples. Since our samples are of unequal sizes, for the case of equal variances, the *t* statistic is given by

pairs of relevant features of the two subject groups are equal. The alternative hypothesis states that the sample mean for the subject group with APOE ε4 genes is lower indicating that the relevant features are more strongly uncorrelated for this group with the genes than the other group without the genes.

Second, voxel-based morphometry (VBM) is used for comparing the texture maps both within and between the two groups. VBM registers every image (texture map) to a standard template, and smoothens it so that each voxel represents an average value of itself and its neighbors. These operations, consequently, enable comparisons across images, voxel by voxel, where the voxel size can be selected suitably based on the application domain. The VBM outputs were then statistically analyzed for significant differences ($p < 0.05$) in their mean values for every relevant feature type again using the two-sample *t* test.

CHAPTER 4: RESULTS AND DISCUSSION

This Chapter is arranged in the following manner. Section 4.1 describes the experimental set-up, Section 4.2 presents the texture feature maps computed from the T_2 MR images, Section 4.3 presents instances of the white matter masked T_2 MR images with regions of interest marked, Section 4.4 discusses the results that enable the identification of relevant and uncorrelated features, and Section 4.5 presents some statistical significant tests to distinguish between the subjects with and without the presence of APOE ε4 genes.

4.1 Experimental Set-Up

Twenty six (26) middle-aged persons in the age group of 45-65 years were used as subjects for the study. They were tested for all forms of dementia and found to be healthy. However, they could be divided into two categories based on whether they possessed the common genes that are observed in AD patients. Fifteen subjects (15) carried the APOE ε3ε4 (fourteen) or ε4ε4 (one) genes, while the remaining eleven (11) subjects did not carry APOE ε4 genes (instead they had ε2ε3 or ε3ε3 genes). We sometimes refer to the two subject group as *carriers* and *non-carriers* respectively. No information about the race, gender, or ethnicity of any of the subjects was available. They were all part of an IRB approved, cross-sectional study going on at the Krasnow Institute in George Mason University, where all the participating subjects provided written

consents. The MRI scanner was a Siemens MAGNETOM Allegra of field strength 3.0 Tesla. The format used to store images was .nii that was developed by the Neuroimaging Informatics Technology Initiative (NIfTI). The dimensions of the T_2 - weighted images for each of the subjects were either 208 X 256 X 42 or 208 X 256 X 34. The texture feature map generation and relevant feature identification code were implemented in MATLAB R2011a. The two-sample *t* test was run using the statistical software package R v3.0.0. VBM was computed using the SPM8 toolbox (SPM 2013). All the processes were run on Centos 6.0 OS in an Intel i7 2620M quad core CPU with 2.7 GHz processor speed and 4 GB of RAM.

4.2 Texture Feature Maps of T_2 MR Images

We now present the raw T_2 MR images and the processed texture feature maps for two representative subjects, one without the APOE genes (Figure 4.1) and the other with the APOE genes (Figure 4.2), to highlight the differences among the images for the two subject types while avoiding redundancy. Each figure shows a set of eleven axial views of the brain, one for the T_2 image and the rest for the ten textural features discussed in the previous Chapter. 0° is chosen as the SDM direction for generating all the features maps.

Certain broad trends are observed from the two Figures. First and foremost, differences are seen in the spatial distributions of gray level intensities in the two sets of images. All the images for the subject with the genes have a higher level of overall brightness with larger regions of lighter intensities as compared to the images for the subject without the genes. Since in the T_2 mode, non-white matter portions of the brain are shown with lighter intensities, the presence of such portions within the white matter

regions indicate the possibility of anomalies in the brains of the subjects with the APOE ε4 genes. These anomalies potentially correspond to abnormal protein growth (amyloid plaque and tau tangles) in the brains of the gene-carrying subject. Furthermore, the differences are more pronounced among the texture feature maps as compared to the original T_2 images, thereby validating the choice of texture analysis for detecting early signs of AD. Last but not the least, the intensity differences are more marked for feature maps corresponding to contrast, correlation, sum average, sum variance, and entropy as compared to the other feature types. Identical trends are found on comparing the mean, standard deviation, and mutual information values for the two subject groups in Section 4.4, enabling us to identify the set of relevant and uncorrelated features that afford the best potentials for detecting AD in its early stages.

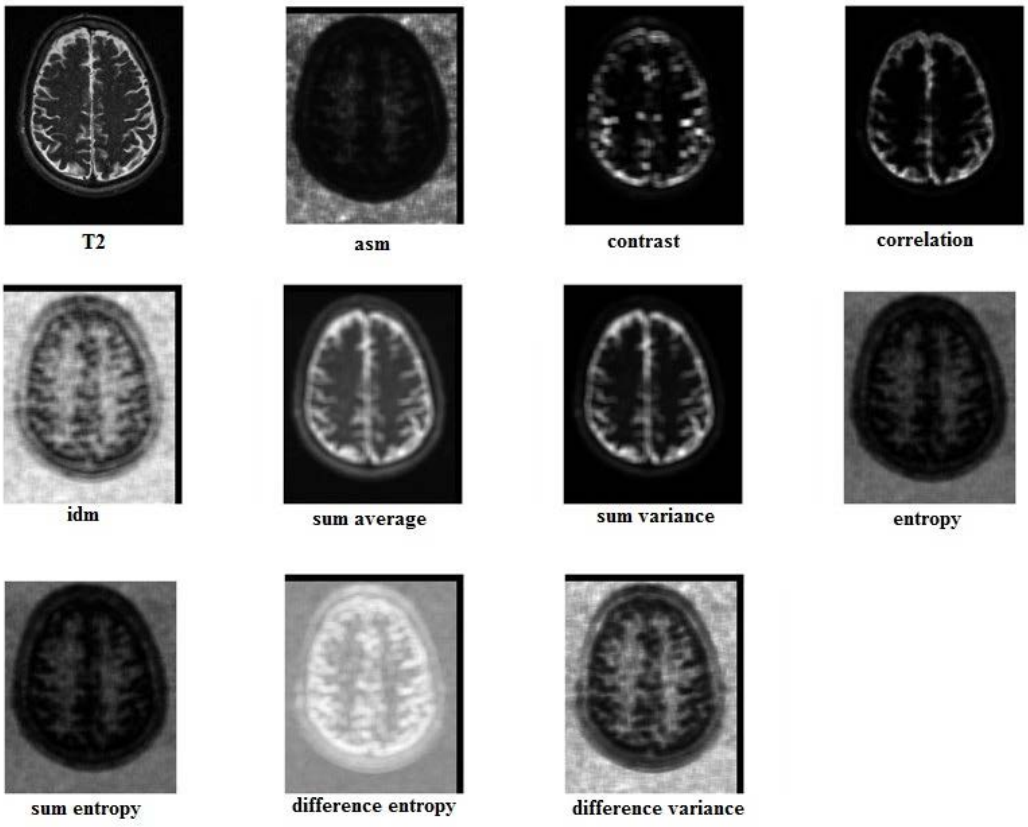

Figure 4.1: Raw T_2 MR Image and processed texture feature maps with SDM direction of 0° for a subject without APOE ε4 genes

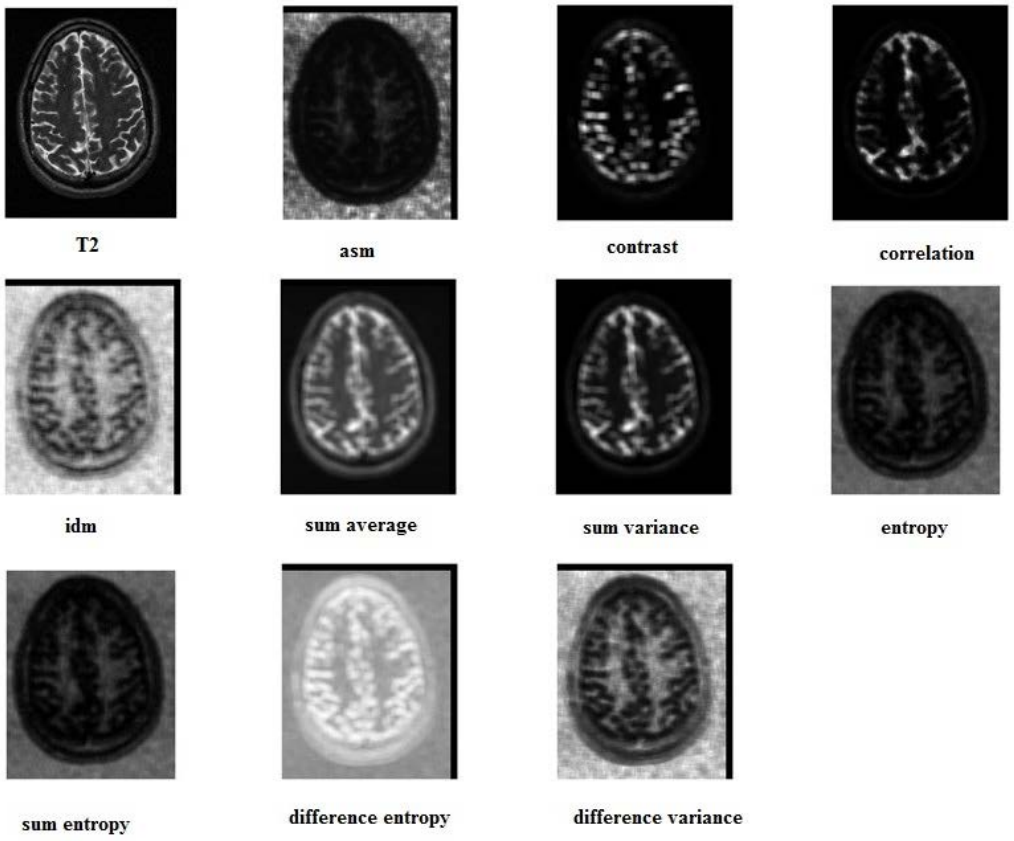

Figure 4.2: Raw T_2 MR Image and processed texture feature maps with SDM direction of 0° for a subject with APOE ε4 genes

Figures 4.3 and 4.4 show the texture maps using correlation (one of the features where marked differences are observed in Figures 4.1 and 4.2) as the feature type for all the four SDM directions of 0°, 45°, 90°, and 135°, and for the same two subjects used earlier. While intensity variations are seen between any two pairs of images corresponding to different subjects, no clear distinctions are observed among the maps

for the same subject with varying SDM directions, indicating that the direction does not play a very important role in causing the intensity differences.

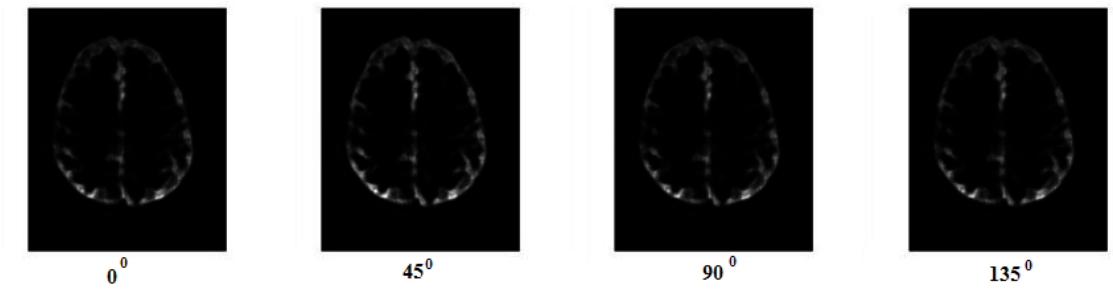

Figure 4.3: Correlation feature maps with varying SDM directions for a subject without APOE ε4 genes

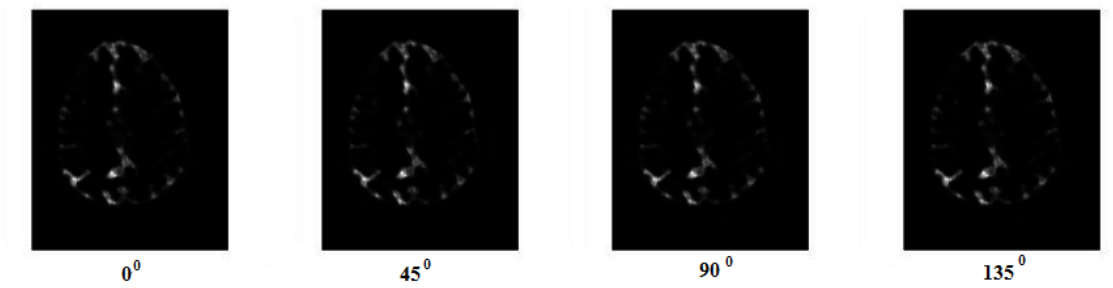

Figure 4.4: Correlation feature maps with varying SDM directions for a subject with APOE ε4 genes

4.3 White Matter Masked T_2 MR Images

As described in Section 4.2, the texture feature maps are computed on the white matter regions of the brain as these regions are usually first affected by AD. To compute these maps, the white matter regions are masked out from the rest of the brain image, and then registered to common brain space to segment the masked image into 50 ROIs based

on the anatomical structures of the brain. The final segmented white matter masked images in the standard MNI brain space (discussed in Section 4.2) are shown in Figure 4.5. Certain ROIs are labeled in the Figure, namely, fornix, left inferior fronto-occipital fasciculus, right uncinate fasciculus, and right and left tapetum corresponding to ROIs 6, 46, 47, 49 and 50 respectively. These ROIs are marked due to the fact that maximum differences in the feature values are observed in these regions as evident from the results presented in the next two Sections.

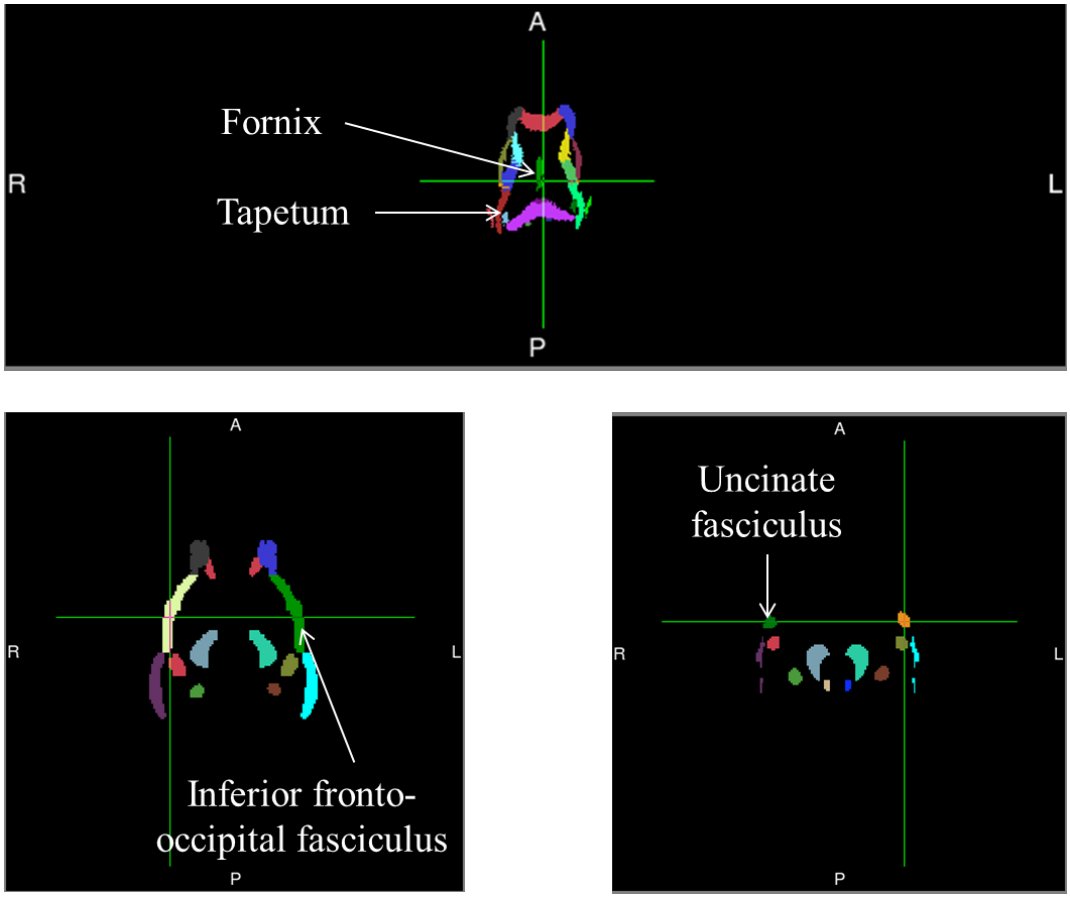

Figure 4.5: White matter regions of interest in standard brain space

4.4 Relevant and Uncorrelated Features for T_2 MR Images

We now present statistical measures of the white matter masked texture feature maps in specific ROIs for the two types of subjects. Tables 4.1 and 4.2 present the mean and standard deviation values of the *relevant* features, namely, contrast, correlation, sum average, sum variance, and entropy, for five ROIs, two SDM directions of 0° and 45°, and a representative subject without the APOE ε4 genes (same one as used earlier). These features are relevant in the sense that they are able to encode useful statistical information about the variations of gray levels in the white matter regions of interest. Several trends are seen from these two Tables. First, the mean values vary substantially among the different ROIs for every feature type. Second, the mean values are quite different from one feature type to another. Third, the mean values vary between the two SDM directions for a given feature type, although this variation is smaller than the variations observed across the feature types. And last, the standard deviation values are less than the mean values, indicating that the variability in capturing the relevant information is smaller than the actual value of the information. Table 4.3 presents the mean values for the other five non-relevant features, namely, ASM, IDM, sum entropy, difference variance, and difference entropy. As opposed to Table 4.1, there are much less (sometimes no) variations in the values from one ROI to another and from one SDM direction to another for s particular feature type, indicating that this feature is not effective in encoding spatial variations in gray level intensities.

Table 4.1: Mean values of relevant features in regions of interest for a subject without APOE ε4 genes

ROI	Features									
	Contrast		Correlation		Sum average		Sum variance		Entropy	
	0°	45°	0°	45°	0°	45°	0°	45°	0°	45°
6	1.24e-8	5.06e-8	0.202	0.207	3.21e-8	2.93e-8	2.4e-6	2.15e-6	1.21e-10	4.15e-10
46	6.45e-9	8.33e-9	0.019	0.019	1.67e-8	1.51e-8	4.59e-7	3.93e-7	2.87e-10	5.86e-10
47	1.13e-8	1.15e-8	0.036	0.038	1.72e-8	1.57e-8	5.33e-7	4.79e-7	2.58e-10	5.41e-10
49	1.78e-8	6.85e-8	0.148	0.153	3.11e-8	2.8e-8	2.5e-8	2.16e-6	2.26e-10	4.99e-10
50	5.15e-9	2.27e-8	0.039	0.034	1.95e-8	1.71e-8	9.26e-7	7.39e-7	3.82e-10	6.38e-10

Table 4.2: Standard deviation values of relevant features in regions of interest for a subject without APOE ε4 genes

ROI	Features									
	Contrast		Correlation		Sum average		Sum variance		Entropy	
	0°	45°	0°	45°	0°	45°	0°	45°	0°	45°
6	7.24E-09	2.63E-08	0.131	0.131	1.22E-08	1.09E-08	1.64E-06	1.47E-06	7.09E-11	5.60E-11
46	4.09E-09	5.37E-09	0.026	0.027	2.75E-09	2.39E-09	2.43E-07	2.01E-07	1.05E-10	8.78E-11
47	7.74E-09	8.04E-09	0.044	0.046	4.12E-09	3.75E-09	3.54E-07	3.23E-07	1.68E-10	1.20E-10
49	1.05E-08	2.78E-08	0.100	0.105	9.34E-09	8.82E-09	1.23E-06	1.16E-06	1.02E-10	8.07E-11
50	2.12E-09	1.34E-08	0.041	0.044	5.59E-09	5.05E-09	6.68E-07	5.82E-07	1.31E-10	1.17E-10

Table 4.3: Mean values of non-relevant features in regions of interest for a subject without APOE ε4 genes

ROI	Features									
	ASM		IDM		Sum entropy		Diff variance		Diff entropy	
	0°	45°	0°	45°	0°	45°	0°	45°	0°	45°
6	3.18E-09	3.17E-09	3.33E-09	3.24E-09	5.99E-09	5.70E-09	3.17E-09	3.17E-09	5.29E-09	5.39E-09
46	3.18E-09	3.18E-09	3.38E-09	3.32E-09	5.71E-09	5.43E-09	3.17E-09	3.17E-09	5.09E-09	5.02E-09
47	3.18E-09	3.18E-09	3.35E-09	3.32E-09	5.76E-09	5.49E-09	3.17E-09	3.17E-09	5.20E-09	5.09E-09
49	3.18E-09	3.18E-09	3.37E-09	3.28E-09	5.89E-09	5.63E-09	3.17E-09	3.17E-09	5.21E-09	5.28E-09
50	3.18E-09	3.18E-09	3.41E-09	3.33E-09	5.70E-09	5.45E-09	3.17E-09	3.17E-09	4.98E-09	5.11E-09

Tables 4.4-4.6 are analogues of Tables 4.1-4.3 with the exception that these Tables present the result for a representative subject with the APOE ε4 genes (same one as used in the Section 4.2). While most of the broad trends in these Tables are identical to those discussed earlier, the actual values vary much more between the two subjects for the relevant features as compared to the other features, demonstrating the potential of the relevant features in distinguishing between the two subject types.

Table 4.4: Mean values of relevant features in regions of interest for a subject with APOE ε4 genes

ROI	Features									
	Contrast		Correlation		Sum average		Sum variance		Entropy	
	0°	45°	0°	45°	0°	45°	0°	45°	0°	45°
6	1.50E-08	4.26E-08	0.213	0.219	3.04E-08	2.80E-08	2.04E-06	1.87E-06	9.62E-11	4.08E-10
46	6.07E-09	9.03E-09	0.015	0.015	1.68E-08	1.52E-08	4.52E-07	3.86E-07	3.90E-10	6.48E-10
47	7.09E-09	6.11E-09	0.008	0.009	1.38E-08	1.27E-08	2.69E-07	2.40E-07	4.42E-10	7.07E-10
49	1.93E-08	6.17E-08	0.172	0.179	2.77E-08	2.54E-08	1.73E-06	1.54E-06	1.40E-10	4.41E-10
50	6.11E-09	1.67E-08	0.032	0.031	1.76E-08	1.55E-08	6.72E-07	5.30E-07	4.15E-10	6.90E-10

Table 4.5: Standard deviation values of relevant features in regions of interest for a subject with APOE ε4 genes

ROI	Features									
	Contrast		Correlation		Sum average		Sum variance		Entropy	
	0°	45°	0°	45°	0°	45°	0°	45°	0°	45°
6	6.44E-09	2.39E-08	0.133	0.137	7.93E-09	7.57E-09	1.11E-06	1.05E-06	4.55E-11	2.95E-11
46	3.77E-09	8.76E-09	0.012	0.011	2.49E-09	2.18E-09	1.98E-07	1.63E-07	1.15E-10	9.26E-11
47	5.06E-09	3.39E-09	0.009	0.011	2.14E-09	1.91E-09	1.30E-07	1.18E-07	2.34E-10	1.97E-10
49	7.18E-09	3.05E-08	0.134	0.135	6.86E-09	6.38E-09	8.37E-07	7.64E-07	9.54E-11	7.42E-11
50	3.74E-09	1.12E-08	0.041	0.043	4.51E-09	4.06E-09	4.80E-07	4.13E-07	1.82E-10	1.55E-10

Table 4.6: Mean values of non-relevant features in regions of interest for a subject with APOE ε4 genes

ROI	Features									
	ASM		IDM		Sum entropy		Diff variance		Diff entropy	
	0°	45°	0°	45°	0°	45°	0°	45°	0°	45°
6	3.25E-09	3.25E-09	3.38E-09	3.33E-09	6.20E-09	5.89E-09	3.25E-09	3.25E-09	5.53E-09	5.53E-09
46	3.25E-09	3.25E-09	3.50E-09	3.43E-09	5.81E-09	5.53E-09	3.25E-09	3.25E-09	5.12E-09	5.03E-09
47	3.25E-09	3.25E-09	3.48E-09	3.43E-09	5.69E-09	5.42E-09	3.25E-09	3.25E-09	5.17E-09	5.04E-09
49	3.25E-09	3.25E-09	3.39E-09	3.33E-09	6.14E-09	5.87E-09	3.25E-09	3.25E-09	5.53E-09	5.53E-09
50	3.25E-09	3.25E-09	3.50E-09	3.42E-09	5.84E-09	5.57E-09	3.25E-09	3.25E-09	5.13E-09	5.17E-09

Figures 4.6-4.14 show the plots of the mean values of the various features for all the 26 subjects that are divided into groups based on the presence and absence of APOE ε4 genes in three regions of interest. Figures 4.6-4.8 are drawn for the fornix region (ROI number 6), Figures 4.9-4.11 are drawn for the left inferior fronto-occipital fasciculus region (ROI number 46), and Figures 4.12-4.11 are drawn for the right uncinate fasciculus region (ROI number 47). The mean values of all the features except correlation and sum variance are shown in the same plot. Correlation and sum variance means are plotted separately due to the orders of magnitude differences in the actual values. The values for the 15 carrier subjects with the APOE ε4 genes are shown with green symbols and the values for the other 11 non-carrier subjects without the genes are depicted with red symbols. Certain key trends are observed in all the Figures. First, the values are dispersed only for contrast, correlation, sum average, and sum variance feature types; for all the other feature types, the values are tightly clustered together indicating that they are

unable to distinguish among the subjects in either of the two regions of interest. Second, the values for the carriers tend to be higher on an average for the relevant feature types where dispersion occurs. This trend indicates the ability of the relevant feature types to distinguish between carrier and non-carrier subject types. And, third, the separation of the values for the two subject types varies based on the relevant feature type and the ROI. For instance, the values are clearly separated for correlation in the fornix region, for contrast and sum variance in the left inferior fronto-occipital fasciculus region, and for contrast and correlation in the right uncinate fasciculus region. These trends are also demonstrated using two-sample *t* test in the next Section.

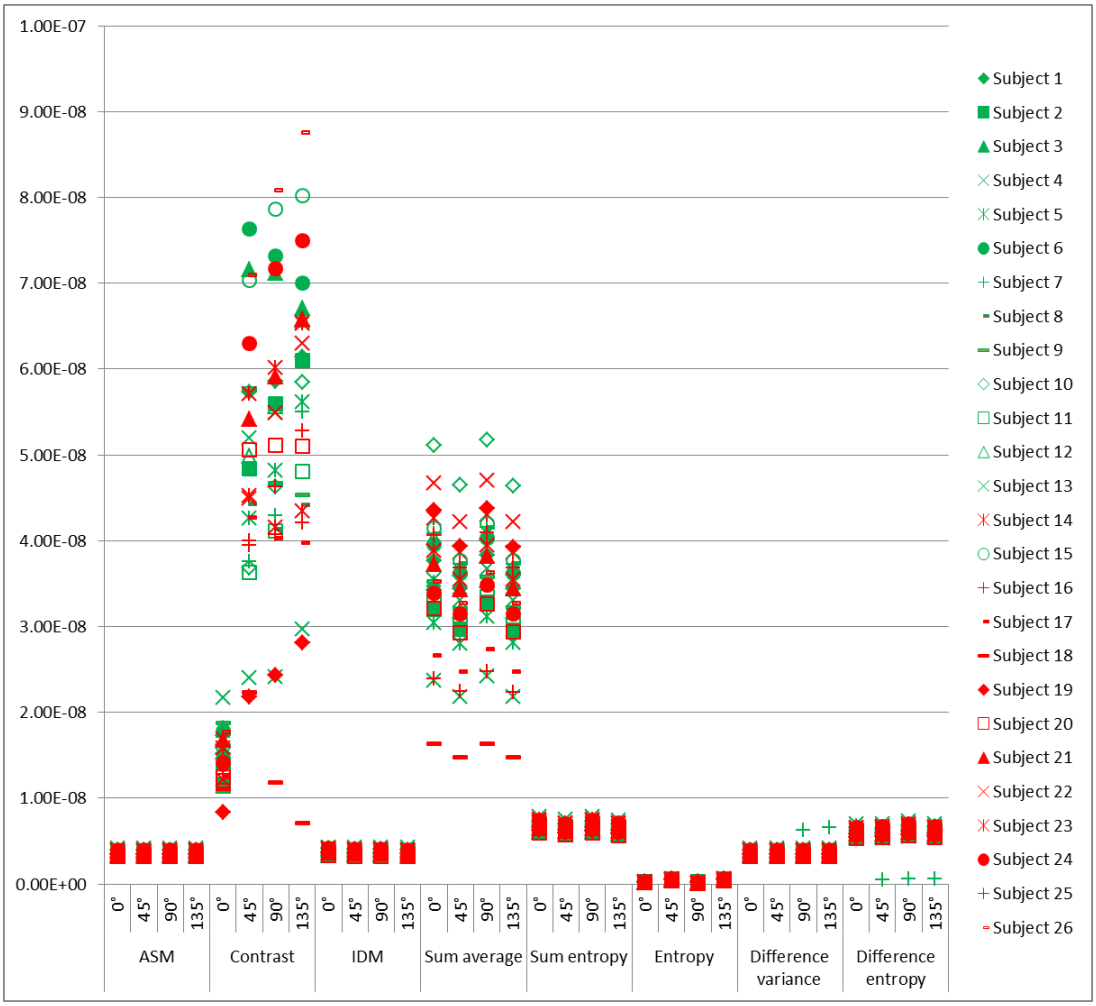

Figure 4.6: Mean values of various features for subjects with and without APOE ε4 genes in fornix region (Green and red indicates non-carriers and carriers respectively.)

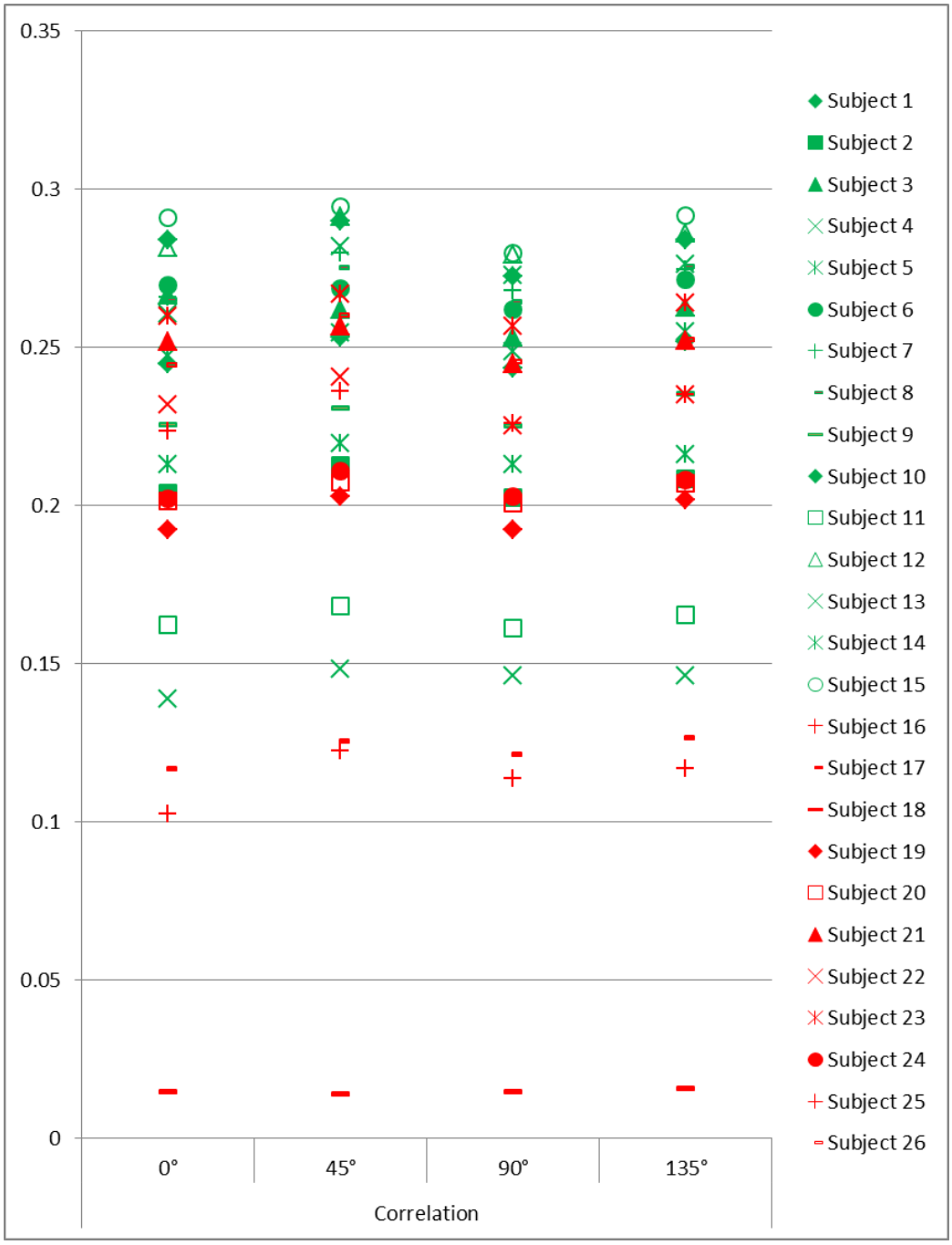

Figure 4.7: Mean values of correlation feature for subjects with and without APOE ε4 genes in fornix region

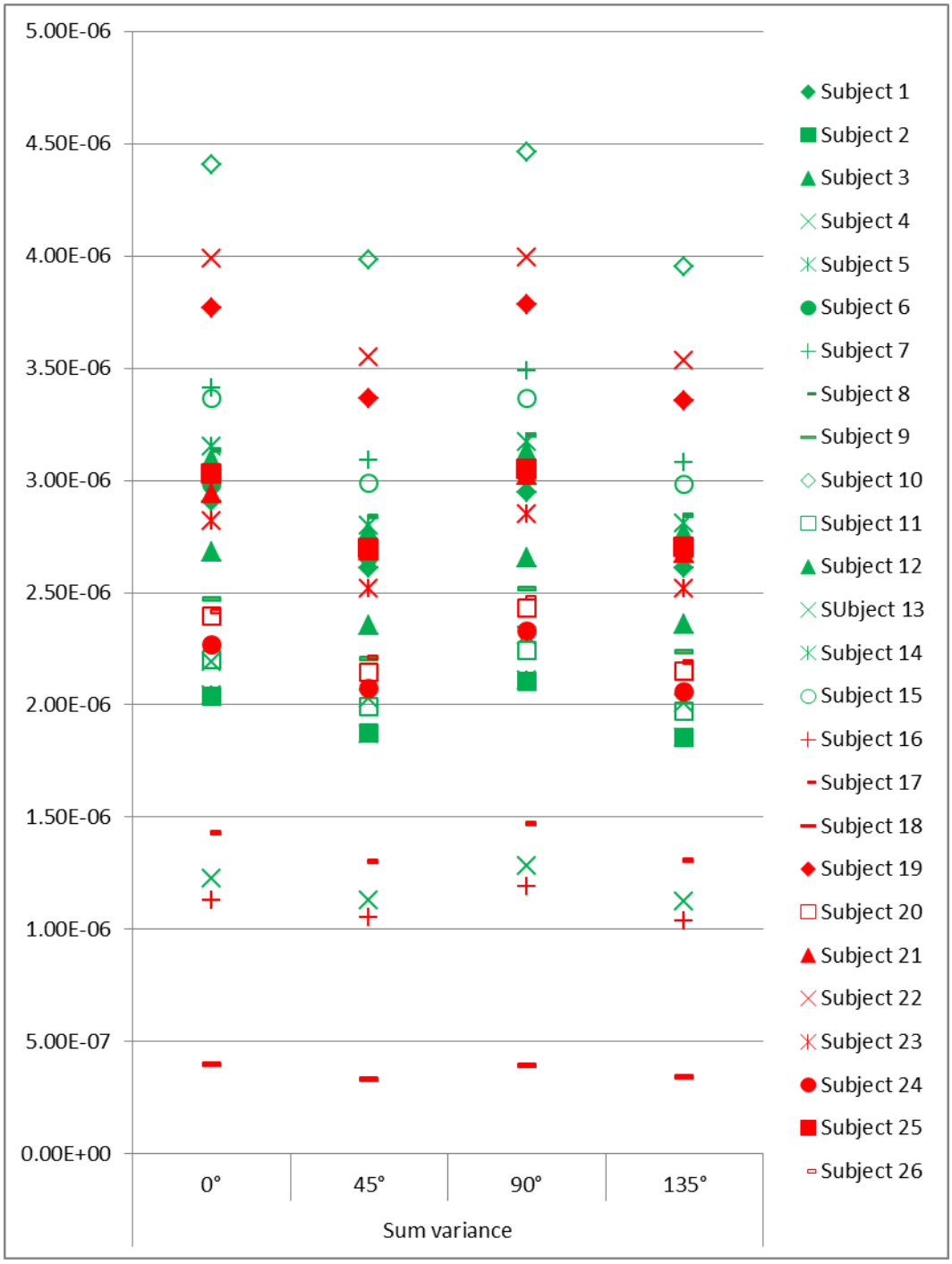

Figure 4.8: Mean values of sum variance feature for subjects with and without APOE ε4 genes in fornix region

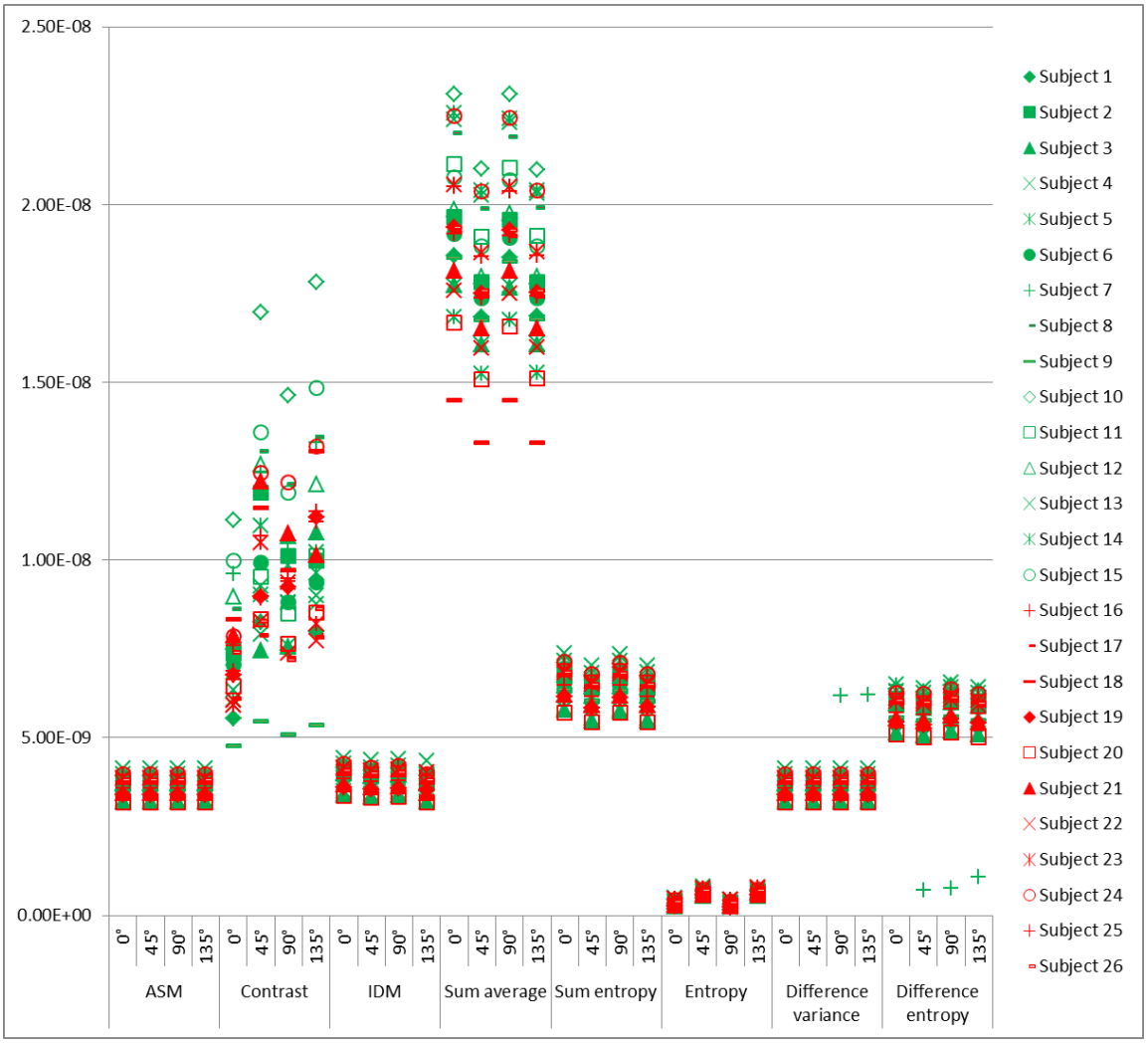

Figure 4.9: Mean values of various features for subjects with and without APOE ε4 genes in left inferior fronto-occipital fasciculus region

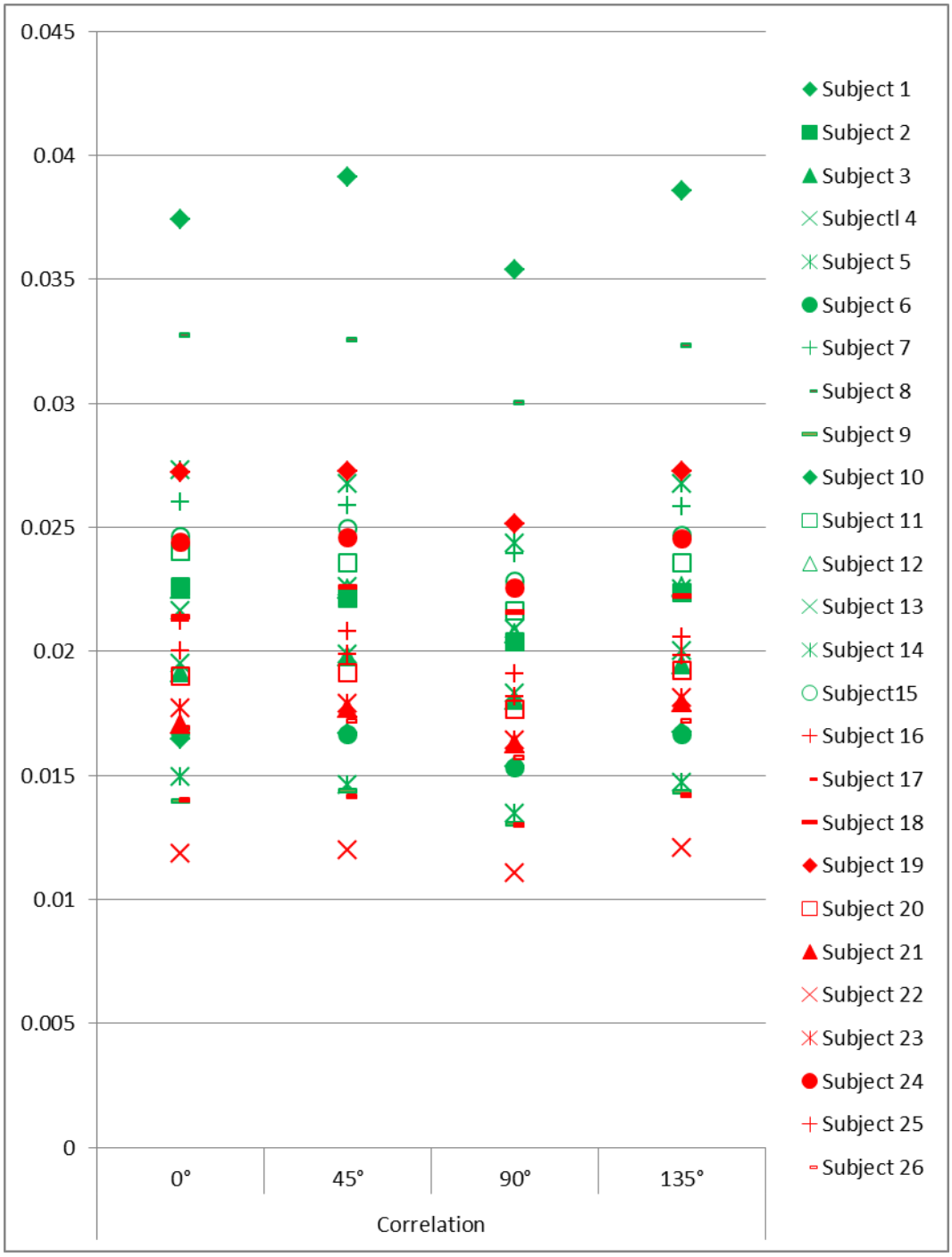

Figure 4.10: Mean values of correlation feature for subjects with and without APOE ε4 genes in left inferior fronto-occipital fasciculus region

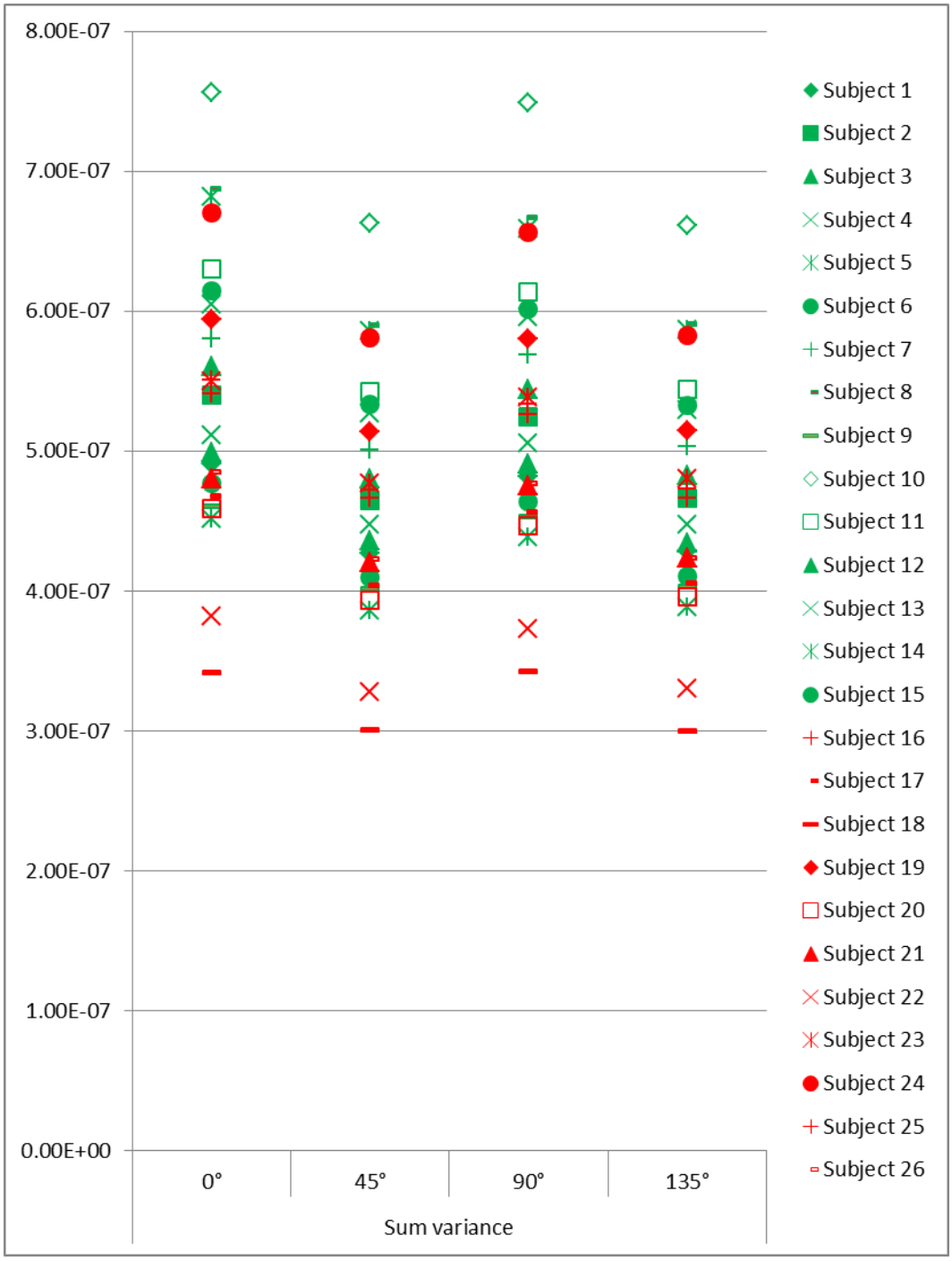

Figure 4.11: Mean values of sum variance feature for subjects with and without APOE ε4 genes in left inferior fronto-occipital fasciculus region

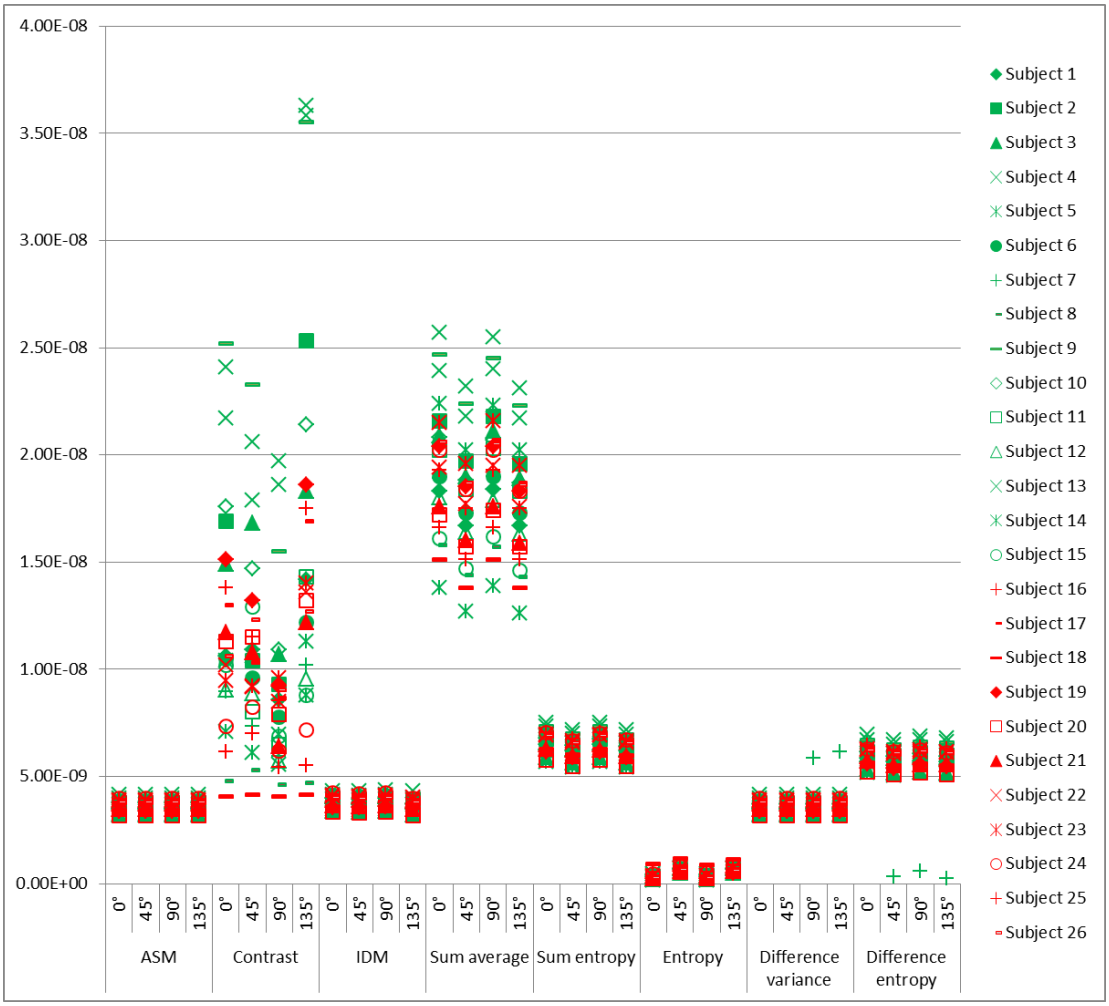

Figure 4.12: Mean values of various features for subjects with and without APOE ε4 genes in right uncinate fasciculus region

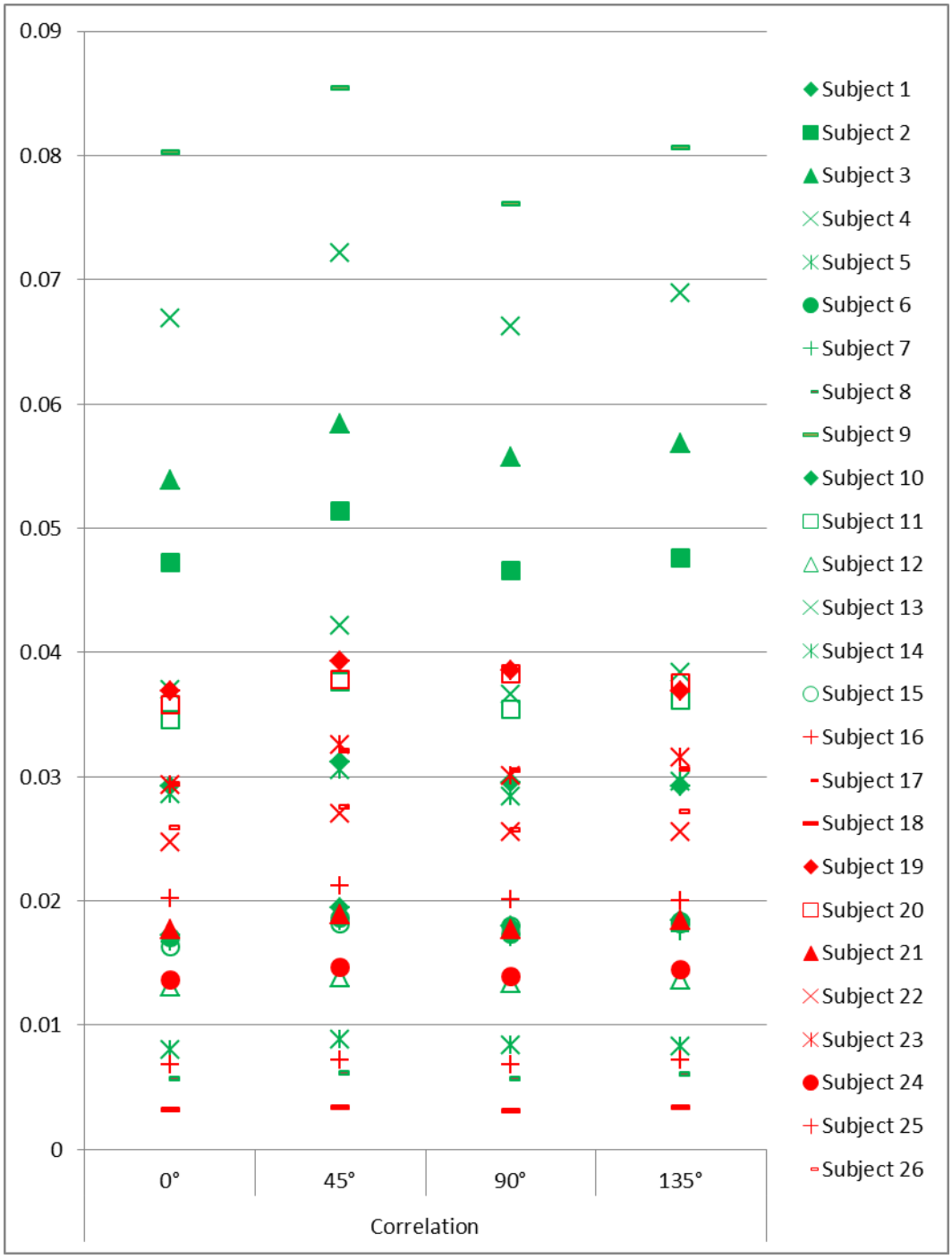

Figure 4.13: Mean values of correlation feature for subjects with and without APOE ε4 genes in right uncinate fasciculus region

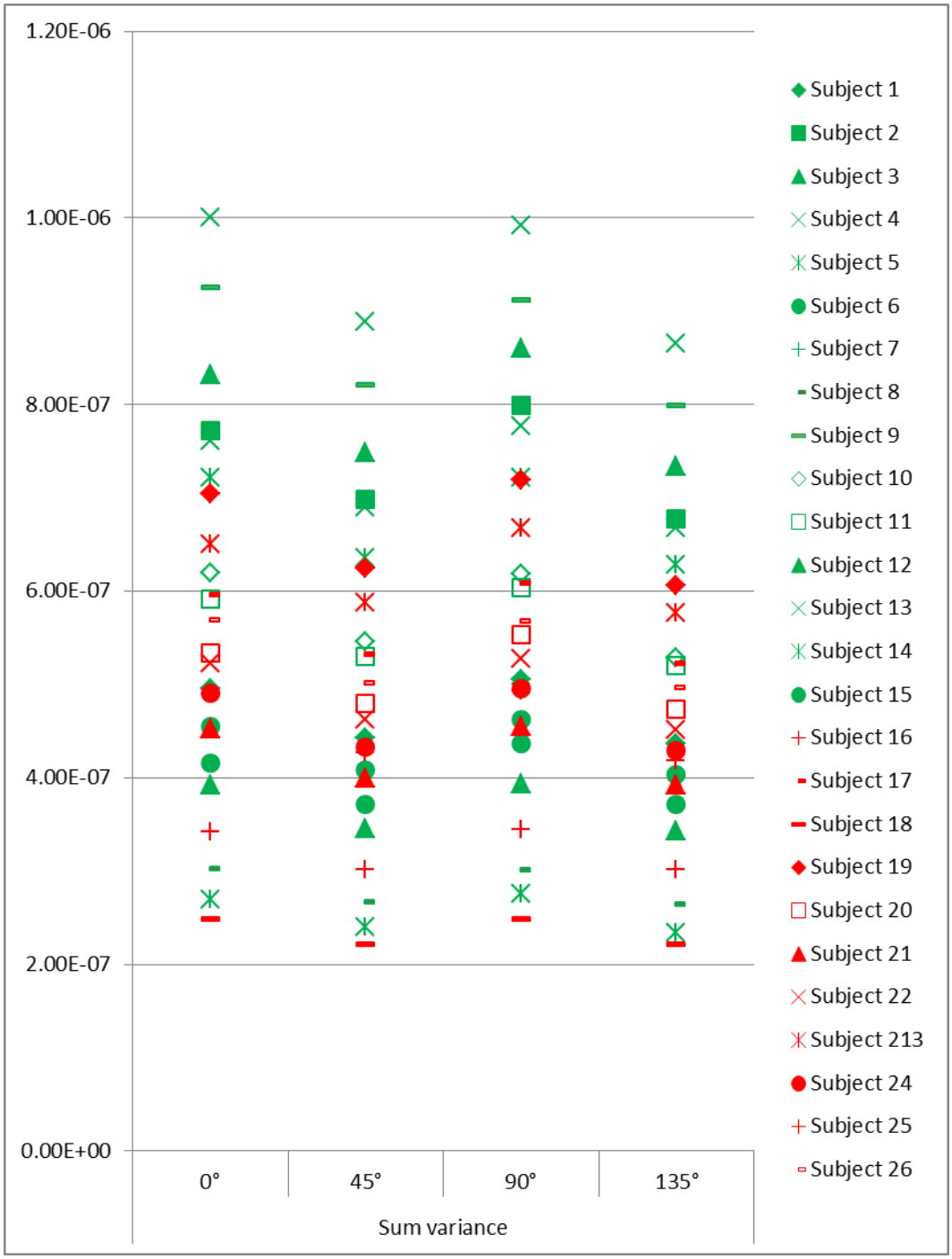

Figure 4.14: Mean values of sum variance feature for subjects with and without APOE ε4 genes in right uncinate fasciculus region

Tables 4.7 and 4.8 show all the mutual information values for pairwise comparison of all the features, both relevant and non-relevant, in a specific ROI numbered 6 and using SDM direction of 0°, for the same two representative subjects used earlier. The values are different in the two tables. While all the values are always greater than 0.001 in the table for the subject without the APOE ε4 genes, 11 pairs of values (marked in bold) are less than 0.001 in the table for the subject with the APOE ε4 genes. Not only does this indicate the ability of the features to distinguish between the two types of subjects (lower values denote greater degree of independence or lack of correlation among the two random variables), these pairs of features correspond to the ones that we have identified as relevant from the feature map images and the mean and standard deviation tables. Thus, our relevant features are also uncorrelated, indicating that this entire set of features is potentially useful in detecting early signs of neurodegeneration.

Table 4.7: Mutual information values for pairwise comparison of features (all 0 degrees) in fornix region for a subject without APOE ε4 genes

	ASM	Contrast	Correlation	IDM	Sum average	Sum variance	Sum entropy	Entropy	Diff variance	Diff entropy
ASM		0.0017	0.0016	0.0018	0.0017	0.0017	0.0018	0.0015	0.0018	0.0018
Contrast			0.0011	0.0020	0.0013	0.0012	0.0020	0.0014	0.0017	0.0021
Correlation				0.0020	0.0011	0.0010	0.0020	0.0013	0.0017	0.0020
IDM					0.0020	0.0020	0.0020	0.0020	0.0017	0.0020
Sum average						0.0012	0.0020	0.0015	0.0017	0.0021
Sum variance							0.0020	0.0013	0.0017	0.0020
Sum entropy								0.0017	0.0018	0.0020
Entropy									0.0015	0.0017
Diff variance										0.0018

Table 4.8: Mutual information values for pairwise comparison of features (all 0 degrees) in fornix region for a subject with APOE ε4 genes

	ASM	Contrast	Correlation	IDM	Sum average	Sum variance	Sum entropy	Entropy	Diff variance	Diff entropy
ASM		0.0012	0.0011	0.0012	0.0012	0.0012	0.0012	0.000974	0.0012	0.0012
Contrast			**0.00042**	0.0013	**0.00053**	**0.0004**	0.0013	**0.000816**	0.0011	0.0013
Correlation				0.0013	**0.00045**	**0.0004**	0.0013	**0.000812**	0.0011	0.0012
IDM					0.0013	0.0013	0.0013	0.001094	0.0012	0.0013
Sum average						**0.00051**	0.0013	**0.000883**	0.0012	0.0013
Sum variance							0.0013	**0.000808**	0.0012	0.0013
Sum entropy								0.0011	0.0012	0.0013
Entropy									**0.0010**	0.0011
Diff variance										0.0012

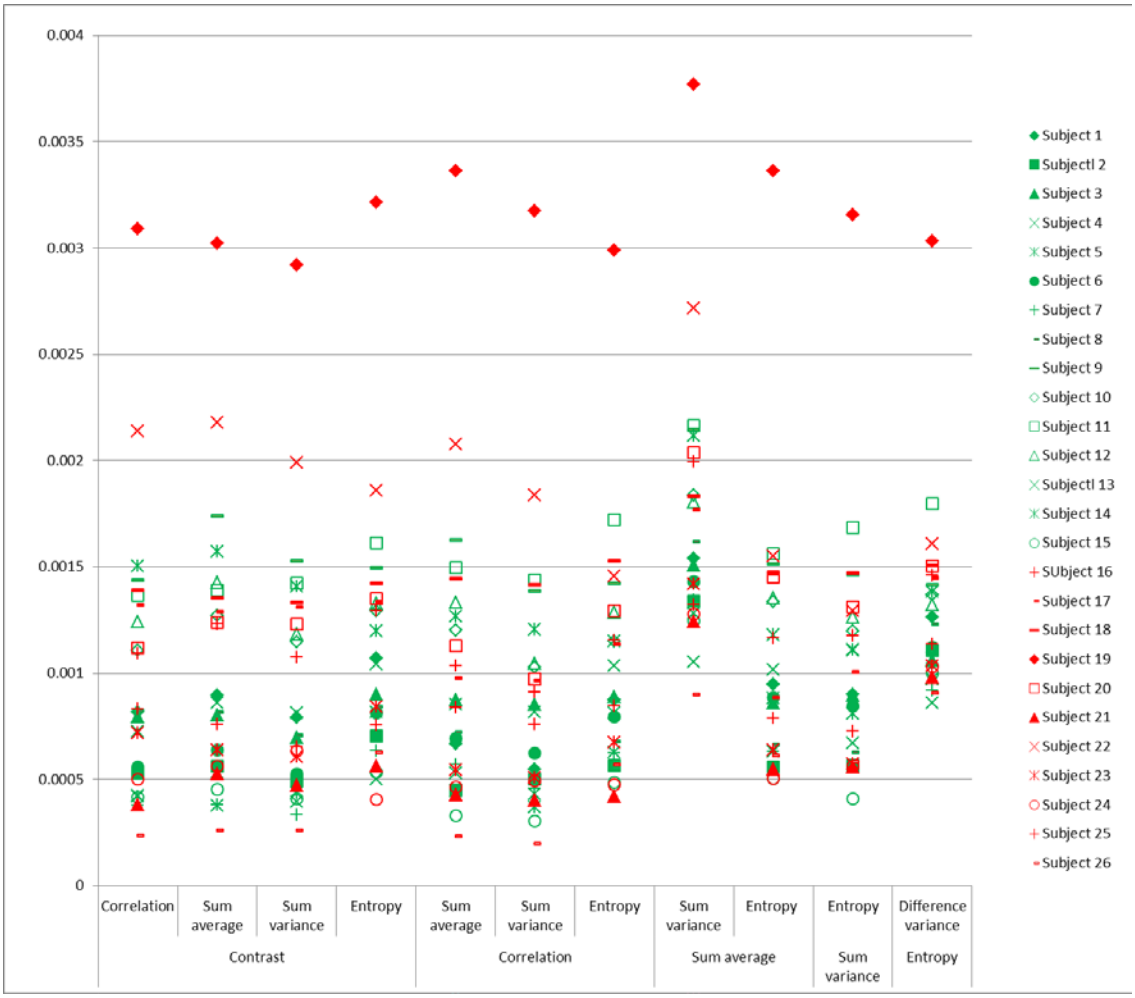

Figure 4.15: Mutual information values of pairs of uncorrelated features for subjects with and without APOE ε4 genes in fornix region

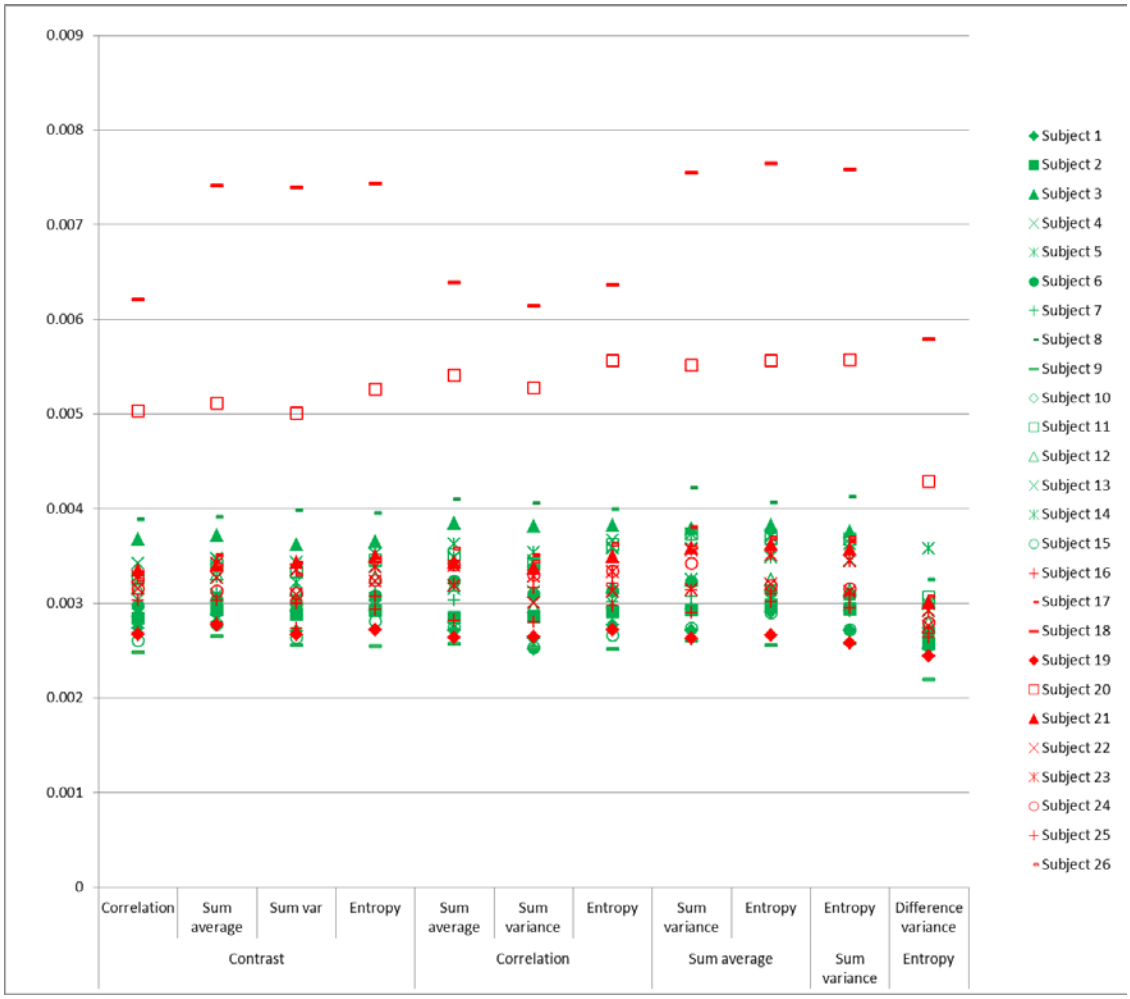

Figure 4.16: Mutual information values of pairs of uncorrelated features for subjects with and without APOE ε4 genes in left inferior fronto-occipital fasciculus region

Figures 4.15 and 4.16 plot the mutual information values of all the pairs of uncorrelated features identified in Table 4.8 for a the subjects in the fornix and the left inferior fronto-occipital fasciculus region respectively. As earlier, the values for the carrier subjects are shown with green symbols, whereas the values for the non-carrier subjects are depicted with red symbols. It is observed that the values for the non-carriers

are higher on an average than the corresponding values for the carriers. Thus, we can conclude that the uncorrelated set of features show a greater degree of independence when they are computed for the carriers, thereby providing the possibility of being able to successfully identify anomalies in the brain for those subjects independent of each other. This trend is corroborated using statistical testing in the next Section.

4.5 Statistical Comparison of Texture Feature Maps for Subjects With and Without APOE ε4 genes

Table 4.9 shows the *p*-values obtained by performing two-sample *t* test on all the subjects that are divided into two groups based on the presence and absence of the APOE genes using the mean values of the relevant features. This testing is done to validate the alternative hypothesis that the two group or sample means are unequal. Indeed, we observe that the *p*-values are less than 0.05 (marked in bold) for certain features in some of the ROIs, and between 0.05 and 0.1 (shown in italicized) in some other cases. It is worthwhile to note here that for all the ROIs there is at least one *p* value that is less than 0.05, indicating that all of them potentially contain early signs of neurodegeneration.

We are able to detect trends and borderline significant results for periventricular ROIs as well as the uncinate fasciculus and the inferior fronto-occipital fasciculus (please note that due to the exploratory nature of the analysis, no correction for multiple comparisons was applied). One needs to take into account the challenges of this analysis – these are neurologically healthy adults, middle aged (45-65 years of age at the time of the scan), long before any potential AD symptoms; additionally, the presence of the ApoE ε4 gene increases the probability, but does not mean that the person will, indeed,

get AD. So, differences, if any, are expected to be very small. Of clinical interest in these results is the uncinate fasciculus, a tract connected to the hippocampus and the last tract to mature in the human brain, both characteristics that make it particularly interesting for AD. Of further clinical significance is the inferior fronto-occipital fasciculus, a tract that together with the uncinate fasciculus has been implicated in aging-related white matter degeneration.(Teipel et al. 2010).

Table 4.9: *p*-values from two sample *t* test on mean values of relevant features for all the subjects with and without APOE ε4 genes in regions of interest

ROI	**Features**									
	Contrast		Correlation		Sum average		Sum variance		Entropy	
	0°	45°	0°	45°	0°	45°	0°	45°	0°	45°
Fornix	**0.031**	0.260	**0.024**	**0.029**	0.166	0.163	0.195	0.192	**0.037**	*0.091*
Left inferior fronto-occipital fasciculus	0.159	0.210	*0.059*	*0.065*	*0.096*	*0.100*	**0.040**	**0.040**	0.283	0.287
Right uncinate fasciculus	**0.048**	*0.068*	*0.087*	*0.079*	0.167	0.163	0.166	*0.096*	0.227	0.200
Right tapetum	*0.053*	**0.025**	0.203	0.194	0.419	0.412	0.484	0.489	*0.078*	0.101
Left tapetum	**0.008**	*0.089*	0.177	0.170	0.118	0.116	0.107	0.103	0.101	0.128

Table 4.10 presents the *p*-values from the two sample *t* test on the pairs of relevant and uncorrelated features that have mutual information values of less than 0.001 as shown in Table 4.8 using the two subject groups, one with APOE ε4 genes and the other without APOE ε4 genes. Based on our hypothesis, if different texture analysis features measure different aspects of heterogeneity that do not change concurrently, then early changes will be strongly reflected in changes in the relationship between them, as

reflected by the mutual information values. While the limited number of subjects does not allow our results to reach formal significance levels, a strong trend for group differences is observed. Several *p* values are between 0.05 and 0.1 and the means for the carrier group are lower than the non-carrier group, indicating a trend of greater independence among the relevant feature pairs in encoding intensity variations in the carrier group. In future, we plan to repeat this analysis using a much larger set of subjects.

Table 4.10: Statistics computed on mutual information values of pairs of relevant features for all the subjects with and without APOE ε4 genes in regions of interest

ROI	**Statistic**	**Relevant feature pairs**					
		Contrast			Correlation		Sum average
		Correlation	Sum average	Sum variance	Sum average	Sum variance	Sum variance
Fornix	Mean, carriers	0.0008	0.0009	0.0008	0.0009	0.0008	0.0016
	Mean, non-carriers	0.0012	0.0012	0.0011	0.0011	0.0011	0.0018
	p value	*0.096*	0.143	*0.095*	0.158	0.123	0.139
Left inferior fronto-occipital fasciculus	Mean, carriers	0.0031	0.0032	0.0031	0.0032	0.0031	0.0033
	Mean, non-carriers	0.0036	0.0037	0.0037	0.0037	0.0036	0.0039
	p value	*0.067*	*0.073*	*0.072*	*0.063*	*0.062*	*0.068*

Figures 4.15 and 4.16 demonstrate what a lower mutual information value means in this context: expansion of the range of values in one variable creates a new populated area on the right side of Figure 4.16 that drops mutual information values. Notice that the creation of an area with a distinct relationship between the two measures occurs in the case of the APOE ε4 carrier. Such changes in the case of texture analysis features are

interesting because they are derived from a single matrix, which makes a certain degree of dependency expected. However, our results demonstrate that there are changes that interfere with this relationship. Furthermore, the presence of such changes that reach statistical significance in the case of small changes, like the ones in our preliminary study, may justify such an analysis as confirmatory result or strengthen the performance of a classifier-based diagnostic system as additional relevant features.

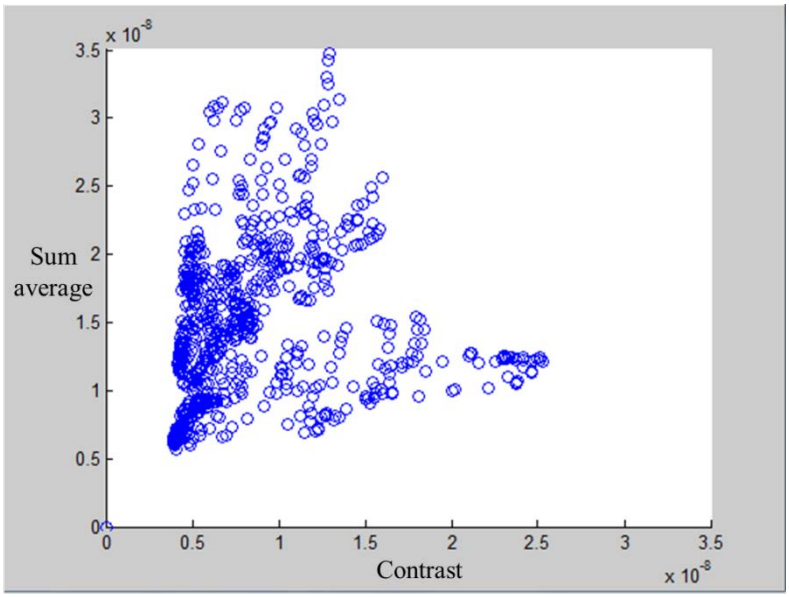

Figure 4.17: Scatter plot of contrast versus sum average features for a subject without APOE ε4 genes in left inferior fronto-occipital fasciculus region

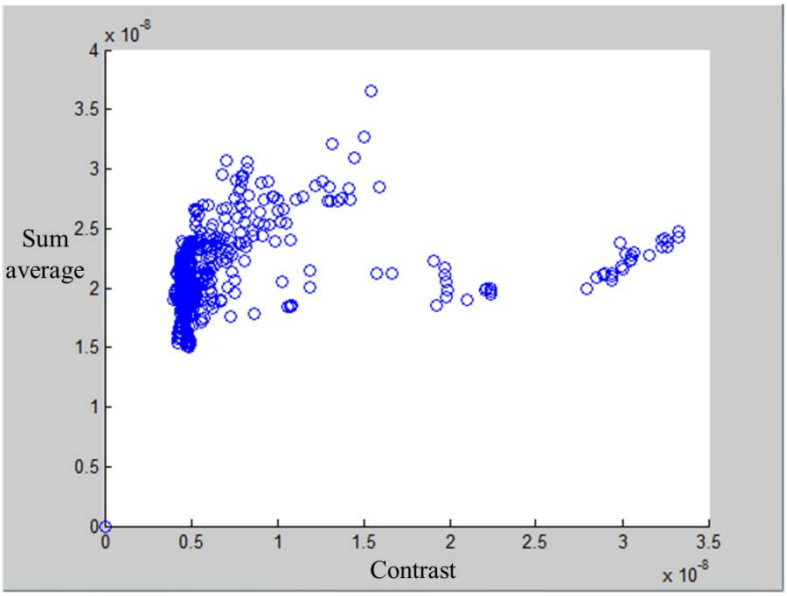

Figure 4.16: Scatter plot of contrast versus sum average features for a subject with APOE ε4 genes in left inferior fronto-occipital fasciculus region

Figures 4.19 shows the VBM result on comparing the two subject groups, one comprising of the APOE ε4 carriers and the other consisting of the non-carriers, using correlation as the texture feature. White matter masking is not employed as the ROIs are automatically identified in this procedure. However, the non-linear registration step described in Section 4.2 is employed to transform every correlation feature map from the T_2 space to the MNI standard brain space. The parameters are set based on the recommended values prescribed in the VBM manual (VBM 2013). Since VBM uses a two-sample *t* test, we need to select a value for *p* (equal to 100% - confidence level) using the familywise error correction method that bounds the number of false positive regions. It is chosen as 0.05. The two groups are assigned contrast values of +1 and -1 respectively. The figure shows a single dark colored region within the white background

of the brain; this region corresponds to a white matter ROI where correlation has been able to detect statistically significant differences between the subject groups. The *p* value in the identified region is lower than the set thresholds and the corresponding *Z* value is greater than 4.5. However, only one such region is identified using VBM unlike in the case of feature means and mutual information values. The other identified regions have high *p* values, and are, thus, deemed to have no statistically significant differences.

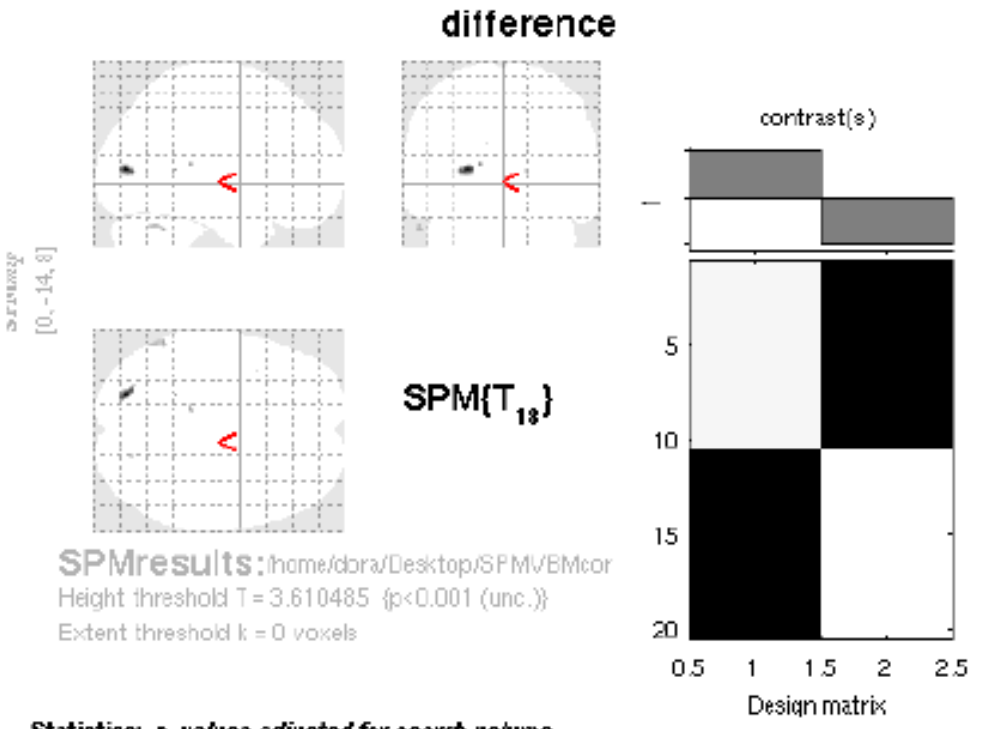

Statistics: ***p-values adjusted for search volume***

set-level		cluster-level				peak-level					mm mm mm		
p	c	$p_{FWE-corr}$	$q_{FDR-corr}$	k	p_{uncorr}	$p_{FWE-corr}$	$q_{FDR-corr}$	T	($Z_=$)	p_{uncorr}			
1.0003		0.953	0.185	293	0.021	0.743	0.119	6.67	4.68	0.000	-23	-79	10
		1.000	0.870	24	0.401	1.000	0.432	5.13	3.98	0.000	-15	-34	13
		1.000	0.870	7	0.725	1.000	0.707	4.52	3.65	0.000	-23	-44	10
		1.000	0.597	110	0.133	1.000	0.707	4.43	3.60	0.000	-58	-53	-30
		1.000	0.870	7	0.725	1.000	0.707	4.12	3.41	0.000	-25	-78	46
		1.000	0.870	16	0.572	1.000	0.707	4.06	3.38	0.000	17	-76	9
		1.000	0.870	2	0.870	1.000	0.707	3.97	3.32	0.000	-10	-98	27
		1.000	0.870	4	0.801	1.000	0.826	3.78	3.20	0.001	-32	-82	40
		1.000	0.870	2	0.870	1.000	0.826	3.75	3.18	0.001	-39	13	-23

table shows 3 local maxima more than 8.0mm apart

Height threshold: T = 3.61, p = 0.001 (1.000) Degrees of freedom = [1.0, 18.0]
Extent threshold: k = 0 voxels, p = 1.000 (1.000) FWHM = 9.0 8.9 8.2 mm mm mm; 9.0 8.9 8.2 {voxels}
Expected voxels per cluster, <k> = 50.909 Volume: 7221032 = 7221032 voxels = 10827.7 resels
Expected number of clusters, <c> = 148.82 Voxel size: 1.0 1.0 1.0 mm mm mm; (resel = 656.57 vox
FWEp: 8.979, FDRp: Inf, FWEc: Inf, FDRc: Inf

Figure 4.19: VBM result on subjects with and without APOE ε4 genes using correlation

CHAPTER 5: CONCLUSIONS

This chapter has been arranged in the following manner. Section 5.1 presents the contributions of this research work. Section 5.2 describes the benefits of the work presented in this thesis. Finally Section 5.3 describes the possible future work in this field.

5.1 Contributions

A new technique to provide the foundation for early detection of Alzheimer's disease (AD) by processing magnetic resonance (MR) images has been presented in this thesis. The major contributions of this work are summarized as follows.

1. *Using textural features to extract meaningful information from T_2 –weighted MR images of subjects with and without APOE ε4 genes*: Texture analysis is used to extract a set of ten statistical features, namely angular second moment, contrast, correlation, inverse difference moment, sum average, sum variance, sum entropy, entropy, difference variance, and difference entropy, that contain information about the spatial distribution of tonal variations in the MR images. Half of the texture feature maps (with a particular feature value for every image voxel) show clear group-wise differences in the gray tonal distributions of the MR images for a majority of the subjects divided into two groups based on the presence and absence of the APOE ε4 genes that are commonly found among AD patients. These group-wise

differences indicate the potential of the corresponding textural features in early identification of the onset of AD.

2. *Improving differentiation between subjects with and without APOE ε4 genes by computing textural feature maps on white matter masked T_2 –weighted MR images segmented into regions of interest*: The white matter regions of the T_2 MR images were segregated from the entire brain by a manual non-linear registration technique to map the T_2 images into a standard brain atlas. This registration also enabled segmentation of the white matter into regions of interest (ROIs) based on the anatomical structure of the brain. The texture feature maps were then computed on just the white matter regions to better capture the group-wise differences in the gray tone distributions among subjects with and without APOE ε4 genes. Enhancement of the differences is consistent with the medical research finding that the early effects of AD are evident in the white matter portions of the brain.
3. *Identifying most relevant and uncorrelated textural features from the overall feature set using statistical measures*: A combination of statistical measures is used to identify the subset of uncorrelated textural features that yield significantly more group-wise differences than the ones that are not included in this subset. In other words, this step enables us to obtain the set of relevant features that can independently provide a good prediction about the early onset of AD. The statistical measures consist of mean, coefficient of variance, and mutual information. The mean is the simplest measure, and yet it is powerful enough to indicate whether a particular feature is able to yield significantly different values from one white matter ROI to

another and from one subject with APOE ε4 genes to another subject without APOE ε4 genes. The coefficient of variance shows whether the variability of the feature that does yield significantly different values is substantially lower than the average indicating that the results are meaningful. Mutual information is utilized to ensure that the relevant features are uncorrelated, thereby establishing the need to retain all the relevant features as potential predictors of the early onset of AD.

4. *Validating the ability of the relevant and uncorrelated textural features to distinguish between subjects with and without APOE ε4 genes using statistical significance tests*: Validation of the ability of the relevant textural features to identify early signs of the onset of AD is done in a surrogate manner by performing statistical hypothesis testing on the two subject groups. The standard two-sample *t* test with unequal sample sizes is used to evaluate whether the sample means of the mean relevant feature values and the mutual information values of the pairs of uncorrelated features are equal for specific ROIs. While the hypotheses testing often lead to inconclusive results when all the subjects are included, they, indeed, show significant differences for a large subset of the subjects. The inconclusive results can be due to the fact that not all of the subjects with APOE ε4 genes have already developed or ever will develop AD. Thus, the overall results are promising in the sense that a certain set of uncorrelated textural features are able to detect early signs of AD (identify true positives) and may also be able to avoid unnecessary diagnosis of subjects without any signs of AD (discard false positives).

5.2 Benefits

Currently, early detection of AD from structural MR images remains a major challenge for the medical research community. According to the AD Report (Alzheimer's Association 2012), more than half of an estimated 5.4 million Americans (of all ages) having AD are not diagnosed properly early enough. Every 1 out of 85 persons is expected to have AD by the year 2050. While researchers are still searching for permanent cures, palliative measures comprising of medications, psychosocial interventions, and assistive caregiving can substantially improve the quality of life of AD patients. Hence, there is an immense need for robust and reliable diagnosis of AD in its early stages to positively affect the lives of millions of people.

Although various image processing techniques like texture analysis, clustering and classification, and voxel-based analysis have shown some promise, none of the techniques has been shown to be capable of addressing the challenge satisfactorily. It is anticipated that this work, which uses texture analysis in conjunction with statistical feature selection and voxel-based morphometry, will provide a feasible path toward overcoming this challenge without requiring genetic information and rather expensive and sometimes inaccessible functional imaging modalities.

5.3 Future Work

While the current work provides a foundation for early detection of AD from T_2 – weighted MR images, further work needs to be done in the following areas to address the problem in its entirety.

1. *Effective feature generation*: A fixed set of textural features is chosen to encode meaningful information from the MR images, and a subset of the chosen set is identified as the potential predictors of the early onset of AD. Thus, feature selection is performed by first defining an initial set based on prior success in image classification and then applying statistical metrics to obtain a smaller set of features with significantly better predictive powers than the others in the initial set. While this feature generation method shows promising results, it is reasonable to believe that the quality of the results can be further enhanced by adopting more involved feature generation approaches. For instance, it may be useful to investigate whether a combination of features (*n*-tuples like pairs or triples) can yield better results. It may also be useful to examine whether feature selection can be combined with feature extraction for generating higher-quality results. In feature extraction, dimensionality reduction techniques such as principal component analysis or shape analysis techniques like Hough transform are used to detect features from raw images, thereby providing a potentially broader and richer set of initial features than the one used in the thesis.
2. *Extensive validation and verification*: While the results in this work are promising, they are sometimes not conclusive. More specifically, even though some of the textural features show statistically significant differences in certain ROIs when a subset of the subjects is divided into two groups, one with APOE ε4 genes and the other without APOE ε4 genes, certain trends cannot be conclusively explained. First, we are unable to fully rationalize why certain features show differences in a particular

ROI, whereas the other uncorrelated features do not show differences in the same ROI but shows differences in some other ROI. Second, we cannot be certain if the lack of significant differences when all the subjects are included is because of the absence of AD in many subjects that have the APOE genes or due to the inherent limitations of the presented technique. Hence, it is imperative to conduct further experimental trials for validating and verifying the technique. Verification will require ground truth knowledge, i.e., accurate information about the actual onset of AD in its early stage in the subjects instead of the surrogate measure of having the APOE genes. For validation, several long-duration trials have to be performed to test whether the subjects, who are predicted to have early symptoms of AD, indeed, get diagnosed for AD after a few months or even years. Further basic clinical research is also needed to obtain strong correlations among white matter ROIs and early stages of AD, which will then enable us to assess the accuracy and general applicability of the predictions of the individual features.

REFERENCES

Aggarwal, N., & Agrawal, R. K. (2012). First and Second Order Statistics Features for Classification of Magnetic Resonance Brain Images. *Journal of Signal and Information Processing,* 3(2): 146-153.

Alzheimer's Association. (2012). 2012 Alzheimer's disease facts and figures. *Alzheimer's & Dementia,* 8(2): 131-168.

Ashburner, J., & Friston, K. J. (2000). Voxel-Based Morphometry—The Methods. *Neuroimage, 11*(6): 805-821.

Bernasconi, A., Antel, S. B., Collins, D. L., Bernasconi, N., Olivier, A., Dubeau, F., Pike, G. B., Andermann, F., & Arnold, D. L. (2001). Texture analysis and morphological processing of magnetic resonance imaging assist detection of focal cortical dysplasia in extra-temporal partial epilepsy. *Annals of Neurology,* 49(6): 770–775.

Butler, P., Mitchell, A. W. M., & Ellis, H. (2007). *Applied Radiological Anatomy for Medical Students*, Cambridge University Press.

Castellano, G., Bonilha, L., Li, L. M., & Cendes, F. (2004). Texture analysis of medical images. *Clinical Radiology,* 59(3): 1061-1069.

Chincarini, A., Bosco, P., Calvini, P., Gemme, G., Esposito, M., Olivieri, C., Luca, R., Sandro, S., Rodriguez, G., Bellotti, R., Cerello, P., Mitri, I. D., Rettico, A., Nobili, F., & the Alzheimer's Disease Neuroimaging Initiative. (2011). Local MRI analysis approach in the diagnosis of early and prodromal Alzheimer's disease. *Neuroimage,* 58(2): 469-480.

Devanand, D. P., Pradhaban, G., Liu, X., Khandji, A., De Santi, S., Segal, S., Rusinek, H., Pelton, G. H., Honig, L. S., Mayeux, R., Stern, Y., Tabert, M. H., & de Leon, M. J. (2007). Hippocampal and entorhinal atrophy in mild cognitive impairment. *Neurology,* 68(11): 828-836.

de Oliveira, M. S., Balthazer, M. L. F., D'Abreu, A., Yasuda, C. L., Damasceno, B. P., Cendes, F., & Castellano, G. (2011). MR Imaging Texture Analysis of the Corpus

Callosum and Thalamus in Amnesic Mild Cognitive Impairment and Mild Alzheimer Disease. *American Journal of Neuroradiology*, 32(1): 60-66.

Dickerson, B. C., Feczko, E., Augustinack, J. C., Pacheco, J., Morris, J. C., Fischl, B., & Buckner, R. L. (2009). Differential effects of aging and Alzheimer's disease on medial temporal lobe cortical thickness and surface area. *Neurobiology of Aging*, 30(3): 432-440.

Duchesne, S., Caroli, A., Geroldi, C., Barillot, C., Frisconi, G. B., & Collins, D. L. (2008). MRI-Based Automated Computer Classification of Probable AD Versus Normal Controls. *IEEE Transactions on Medical Imaging*, 27(4): 509-520.

Estella, F., Delgado-Marquez, B. L., Rojas, P., Valenzuela, O., Roman, B. S., & Rogas, I. (2012). Advanced System for Automously Classify Brain MRI in Neurodegenerative Disease. *Proceedings of IEEE International Symposium on Computer-Based Medical Systems*, Tangiers, Morocco, 250-255.

Farrer, L.A., Cupples, L.A., Haines, J.L., Hyman, B., Kukull, W.A., Mayeux, R., Myers, R.H., Pericak-Vance, M.A., Risch, N., & van Duijn, C.N. (1997). Effects of age, sex, and ethnicity on the association between apolipoprotein E genotype and Alzheimer's disease: a meta-analysis. *The Journal of the American Medical Association*, 278(16): 1349-1356.

Gold, B. T., Johnson, N. F., Powell, D. K., & Smith, C. D. (2012). White matter integrity and vulnerability to Alzheimer's disease: Preliminary findings and future directions. *Biochimica et Biophysica Acta*, 1812(3): 416-422.

Haralick, R. M., Shanmugam, K., & Dinstein, I. (1973). Textural Features for Image Classification. *IEEE Transactions on Systems, Man, and Cybernetics*, 3(6): 610-621.

Heckemann, R. A., Keihaninejad, S., Aljabar, P., Gray, K. R., Nielsen, C., Rueckert, D., Hajnal, J. V., Hammers, A., & the Alzheimer's Disease Neuroimaging Initiative. (2011). Automatic morphometry in Alzheimer's disease and mild cognitive impairment. *Neuroimage*, 56(4): 2024-2037.

Herlidou, S., Rolland. Y., Bansard, J. Y., Le Rumeur, E., & De Certaines, J. D. (1999), Comparison of automated and visual texture analysis in MRI: characterization of normal and diseased skeletal muscle. *Magnetic Resonance Imaging*, 17(9): 1393–1397.

Ikonomidou, V., Stern, S., Gallo, A., Evangelou, I., Ohayon, J., Ehrmantraut, M., Cortese, I., Frantzis, C., McFarland, H., Kane, R., &. Bagnato, F. (2008), Detecting diffuse white matter alterations in healthy volunteers using Tissue

Specific Imaging: Potential implications for cognitive function, *Scientific Meeting and Exhibition of the International Society for Magnetic Resonance in Medicine*, Toronto, Canada

Jack, C. R., Lowe, V. J., Weigand, S. D., Wiste, H. J., Senjem, M. L., Knopman, D.S., Shiung, M. M., Gunter, J. L., Boeve, B. F., Kemp, B. J., Weiner, M., Peterson, R. C., & The Alzheimer's Disease Neuroimaging Initiative (2009). Serial PIB and MRI in normal, mild cognitive impairment and Alzheimer's disease: implications for sequence of pathological events in Alzheimer's disease. *Brain,* 132(Pt 5): 1355-1365.

Jenkinson, M., & Smith, S. M. (2001). A global optimisation method for robust affine registration of brain images. *Medical Image Analysis*, 5(2): 143-156.

Jenkinson, M., Bannister, P. R., Brady, J. M., & Smith, S. M. (2002). Improved optimisation for the robust and accurate linear registration and motion correction of brain images. *Neuroimage,* 17(2): 825-841.

Jenkinson, M., Beckmann, C. F., Behrens, T. E., Woolrich, M. W., & Smith, S. M. (2012). FSL. *Neuroimage,* 62(4): 782-790.

Kassner, A., & Thornhill, R. E. (2010). Texture Analysis: A Review of Neurologic MR Imaging Applications. *American Journal of Neuroradiology,* 31(5): 809-816.

Li, X, Xia, H., Zhou, Z., & Tong, L. (2010). Study on Texture Characteristics of Hippocampus in MR Images of Patients with Alzheimer's Disease. *Proceedings of IEEE International Conference on Biomedical Engineering and Informatics*, Yantai, China, 1-4.

ICBM (2013), http://www.loni.ucla.edu/Atlases/Atlas_Methods.jsp?atlas_id=15, retrieved 3/27/2013.

Mahmoud-Ghoneim, D., Toussaint, G., Constans, J. M., De Certaines, J. D. (2003). Three dimensional texture analysis in MRI: a preliminary evaluation in gliomas. *Magnetic Resonance Imaging*, 21(9): 983–987.

McAuliffe, M. J., Lalonde, F. M., McGarry, D., Gandler, W., Csaky, K., & Trus, B. L. (2001). Medical Image Processing, Analysis & Visualization In Clinical Research. *Proceedings of IEEE International Symposium on Computer-Based Medical Systems,* Bethesda, MD, USA, 381-386.

Muskulus, M., Scheenstra, A. E. H., Braakman, N., Dijkstra, J., Verduyn-Lunel, S., Alia, A., de Groot, H. J. M., & Reiber, J. H. C. (2009). Prospects for Early Detection of

Alzheimer's Disease from Serial MR Images in Transgenic Mouse Models. *Current Alzheimer Research*, 6(6): 503-518.

NIA (2013), http://www.nia.nih.gov/alzheimers/publication/alzheimers-disease-fact-sheet, retrieved 6/16/2013.

NIA Genetics (2013), http://www.nia.nih.gov/alzheimers/publication/alzheimers-disease-genetics-fact-sheet, retrieved 7/8/2013.

NIA Medication (2013), http://www.nia.nih.gov/alzheimers/publication/alzheimers-disease-medications-fact-sheet, retrieved 7/8/2013.

Paulsen, J. S., Nopoulos, P. C., Eylward, A., Ross, C. A., Johnson, H., Magnotta, V. A., Juhl, A., Pierson, R. K., Mills, J., Langbehn, D., Nance, M., & the PREDICT-HD Investigators and Coordinators of the Huntington's Study Group (2010). Striatal and white matter predictors of estimated diagnosis for Huntington disease. *Brain Research Bulletin*, 82(3-4): 201-207.

Schuff, N., Woerner N., Boreta, L., Kornfield, T., Shaw, L. M., Trojanoswki, J. Q., Thompson, P. M., Jack, C. R., Weiner, M. W., & the Alzheimer's Disease Neuroimaging Initiative (2009). MRI of hippocampal volume loss in early Alzheimer's disease in relation to ApoE genotype and biomarkers. *Brain*, 132(Pt 4): 1067-1077.

Smith, C. D., Chebrolu, H., Andersen, A. H, Powell, D. A., Lovell, M. A., Xiong, S., & Gold, B. T. (2010). White matter diffusion alterations in normal women at risk of Alzheimer's disease. *Neurobiology of Aging*, 31(3): 1122-1131.

Smith, S.M. (2002). Fast robust automated brain extraction. *Human Brain Mapping*, 17(3): 143-155.

SPM (2013), http://www.fil.ion.ucl.ac.uk/spm/, retrieved 3/27/2013.

Stricker, N. H., Schweinsburg, B. C., Delano-Wood, L., Wierenga, C. E., Bangen, K. J., Haaland, K. Y., Frank, L. R., Salmon, D. P., & Bondi, M. W. (2009). Decreased white matter integrity in late-myelinating fiber pathways in Alzheimer's disease supports retrogenesis. *Neuroimage*, 45(1): 10-16.

Teipel, S.J., Meindl, T., Wagner, M., Steilties, B., Reuter, S., Hauenstein, K.H., Filippi, M., Ememann, U., Reiser, M.F., & Hampel, H. (2010). Longitudinal changes in fiber tract integrity in healthy aging and mild cognitive impairment: a DTI follow-up study. *Journal of Alzheimer's Disease*, 22(2): 507-522.

VBM (2013), www.fil.ion.ucl.ac.uk/~john/misc/VBMclass10.pdf, retrieved 7/15/2013.

Wang, X, Yang, H., Tong, L., & Liu, W. (2012). MR Image Texture analysis of the Corpus Callosum in Different Gender Patients with Alzheimer's disease. *Proceedings of International Conference on Intelligent Control and Information Processing,* Dalian, China, 290-292.

Zarei, M., Patenaude, B., Damoiseaux, J., Morgese, C., Smith, S., Matthews, P. M., Barkhof, F., Rombouts, S., Sanz-Arigita, E., & Jenkinson, M. (2010). Combining shape and connectivity analysis: An MRI study of thalamic degeneration in Alzheimer's disease. *Neuroimage,* 49(1): 1-8.

Zhang, D., Wang, Y., Zhou, L., Yuan, H., Shen, D., & the Alzheimer's Disease Neuroimaging Initiative (2011). Combining shape and connectivity analysis: An MRI study of thalamic degeneration in Alzheimer's disease. *Neuroimage,* 55(3): 856-867.

Zhang, Y., Schuff, N., Du, A-T., Rosen, H. J., Kramer, J. H., Gorno-Tempini, M. L., Miller, B. L., & Weiner, M. W. (2009). White matter damage in frontotemporal dementia and Alzheimer's disease measured by diffusion MRI. *Brain,* 132(Pt 9): 2579-2592.

Zhang, Y., Brown, L., & Metz, L.M. (2013). MRI Texture Spectral Similarity Detects White Matter Microstructure as Compared to Diffusion Tensor Imaging. *The International Society for Magnetic Resonance in Medicine Annual Meeting & Exhibition*, Salt Lake City, UT, USA.

Zhou, X, Liu, Z., Zhou, Z., & Xia, H. (2010). Study on Texture Characteristics of Hippocampus in MR Images of Patients with Alzheimer's Disease. *Proceedings of IEEE International Conference on Biomedical Engineering and Informatics,* Yantai, China, 593-596.

CURRICULUM VITAE

Debosmita Biswas received her Bachelor of Engineering in Electrical Engineering from Mumbai University, India, in 2008. She worked as an engineer at Shree N M Electrical Limited and then as a lecturer in K. J. Somaiya Polytechnic, Mumbai, India, before joining George Mason University a graduate student in the fall of 2010. She was a graduate teaching assistant for the past two and a half years.